Modeling Framework for Cost Optimization of Process-Scale Desalination Systems with Mineral Scaling and Precipitation

Oluwamayowa O. Amusat, Adam A. Atia, Alexander V. Dudchenko, and Timothy V. Bartholomew*

Cite This: *ACS EST Engg.* 2024, 4, 1028−1047

Read Online

ACCESS | Metrics & More | Article Recommendations | SI Supporting Information

ABSTRACT: Cost-optimization models are powerful tools for evaluating emerging water treatment processes. However, to date, optimization models do not incorporate detailed chemical reaction phenomena, limiting the assessment of pretreatment and mineral scaling. Moreover, novel approaches for high-salinity and high-recovery desalination are typically proposed without direct quantification of pretreatment needs or mineral scaling. This work addresses a critical gap in the literature by presenting a modeling framework that includes complex water chemistry predictions with process-scale optimization. We use this approach to conduct a technoeconomic assessment on a conceptual high-recovery treatment train that includes chemical pretreatment (i.e., soda ash softening and recarbonation) and membrane-based desalination (i.e., standard and high-pressure reverse osmosis). We demonstrate how to develop and integrate accurate multidimensional surrogate models for predicting precipitation, pH, and mineral scaling tendencies. Our findings show that cost-optimal results balance the costs of pretreatment with reverse osmosis system design. Optimizing across a range of water recoveries (i.e., 50−90%) reveals multiple cost-optimal schemas that vary the chemical dosing in pretreatment and the design and operation of reverse osmosis. Our results reveal that pretreatment costs can be more than double the cost of the primary desalination process at high recoveries due to the extensive pretreatment required to control scaling. This work emphasizes the importance of and provides a framework for including chemistry and mineral scaling predictions in the evaluation of emerging technologies in high-recovery desalination.

KEYWORDS: *pretreatment, mineral scaling, desalination, technoeconomic, optimization*
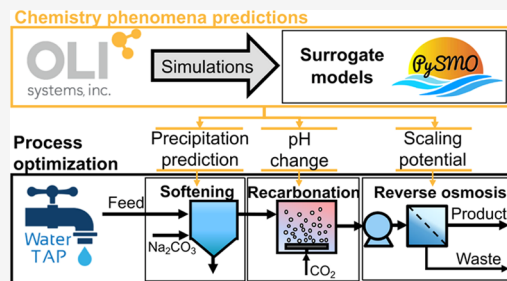
1. INTRODUCTION

Mineral scaling presents a critical challenge for high-recovery desalination because the deposition of mineral solids on surfaces degrades membrane performance, increases thermal resistance in heat exchangers, and damages other equipment.[1−5] Mineral scaling is inherently linked to high-recovery desalination because minerals eventually precipitate when the concentrations of solutes reach solubility as water is extracted and brine is concentrated. This phenomenon typically limits the overall water recovery of desalination processes,[6] resulting in a large generation of waste brine and limiting treatment of saline waters to areas near the coast where brine disposal is cost-effective.[7−9] Thus, broadening the application of desalination will require the design of treatment trains that can operate at higher water recoveries.

Enabling high recovery in desalination processes is challenging since the severity and type of mineral scale depend on the feedwater source and treatment process, requiring a holistic approach to treatment train design. This approach needs to balance cost-trade-offs between the primary desalination processes that yield product water and the pretreatment processes that reduce the scaling potential of the feed. Typically, pretreatment includes chemical precipitation to remove undesirable ions and the addition of

antiscalants that retard the onset of nucleation and crystal growth.[10] These pretreatment processes can significantly increase capital (e.g., precipitation reactors) and operating costs (e.g., chemical addition) depending on the feedwater composition. Some of the pretreatment requirements can be reduced through changes to the design of the desalination process. For example, increasing cross-flow velocity and reducing water flux in reverse osmosis (RO) can minimize scaling potential near the membrane surface by reducing concentration polarization but at a higher capital (e.g., larger membrane areas) and operating cost (e.g., increased pumping and pressure drop). While there has been an extensive effort in conceptualizing and modeling emerging technologies for high-recovery desalination,[11] there is a need to develop frameworks to optimize high-recovery treatment trains across many decision variables while accounting for mineral scaling.

Significant progress has been made over the last two decades in improving the fundamental understanding of mineral scaling phenomena through the development of detailed models and experimental observations. The models focus on estimating thermodynamic solution equilibrium, which can estimate the scaling tendencies of a solution (i.e., estimating whether precipitation will occur). Scaling tendency (ST) is a quantitative measure of the degree of saturation of a solution, and a scaling tendency above one suggests that the solution is supersaturated with respect to a given mineral and solids will form.[1] Modeling approaches for the prediction of scaling tendency range from theoretical to semiempirical models,[12] such as activity coefficient models proposed by Pitzer et al.,[13−17] the electrolyte nonrandom two-liquid model (eNRTL),[18] and the mixed-solvent-electrolyte (MSE) model.[19−22] Additionally, a significant number of experimental studies have been performed on measuring and characterizing mineral scaling under various conditions. Nucleation induction times can be experimentally determined as a function of supersaturation based on classical nucleation theory.[23−26] Experimental investigation of the scaling propensity, specifically in RO applications, has also been widely documented. In one example, a laboratory procedure was proposed for measuring flux decline while recycling concentrate to increase supersaturation over time.[27] Results of this procedure were verified against field data to relate the supersaturation of calcium carbonate to water recovery limits and the effectiveness of antiscalants. In other work, gypsum scaling in RO was characterized through various techniques, such as quantifying the coverage area of crystals on the membrane surface via ex-situ high-contrast imaging,[28,29] assessing axial variation of membrane-surface crystallization via scanning electron microscope (SEM) imaging,[30] and using a quartz crystal microbalance in tandem with SEM imaging to investigate effects of polymeric surface characteristics on crystal formation.[31] Real-time imaging has also been applied to approximate induction time and monitor scale formation on RO membranes as a function of scaling tendency over time.[32−36] Other works have focused on the effects of recovery rate, hydrodynamics, and addition of antiscalants on induction time and scaling of RO membranes.[37−41] Most of these works have focused on developing methods to characterize and predict mineral scaling phenomena for conventional RO applications. However, process-scale models that incorporate mineral-scale predictions and aqueous chemistry calculations can aid in the exploration and early prioritization of new experimental designs for evaluating conceptual and emerging high-recovery systems.

Although there have been great advances in predictive models relevant to mineral scaling in membrane desalination, their application in technoeconomic and process-scale optimization models has been limited, especially with regard to emerging technologies for high-recovery desalination. Many efforts have been focused on incorporating mineral scaling models in bench-scale modules ranging from simple one-dimensional process-scale models to full computational fluid dynamic models relying on either complex mineral scaling models or simple regressions.[42−48] Some models have considered scaling limitations on RO systems, but they do not perform full treatment train optimization.[49] Models of mineral scaling have been rarely used for the cost optimization of treatment trains at the full system scale, with some studies estimating pretreatment costs from pilot scale data,[50−52]

estimating costs from operational data,[53,54] and estimating basic pretreatment design from single dimensional regression.[55] Critically, to our knowledge, the direct incorporation of mineral scaling predictions with rigorous mathematical cost optimization of chemical dosing and RO design in conceptual, high-recovery treatment trains that surpass conventional limitations has never been demonstrated.

Equation-oriented (EO) programming is a powerful tool for the mathematical optimization of complex process systems such as emerging desalination technologies like osmotically assisted RO, membrane distillation, and low-salt-rejection RO.[56−60] However, none of these cost-optimization studies consider chemical phenomena for aqueous solutions, such as precipitation and mineral scaling. Software such as OLI Systems[61] and PHREEQC[62] enable accurate estimation of solution chemistry across a broad range of feed compositions. Such capabilities are especially critical for modeling high-recovery desalination systems, which require predicting mineral scaling tendencies of multicomponent solutions at high ionic strengths and ensuring the process operates below a scaling tendency of one where no solids form thermodynamically. However, EO solvers require access to the modeling equations and their derivatives, and direct calls to external software such as OLI Systems and PHREEQC cannot provide that information. While EO modeling could directly incorporate semiempirical water chemistry models (e.g., Pitzer, eNRTL, MSE, etc.), the complexity, stability, and data requirements of these models have thus far impeded their use in EO analyses.

This work presents the first modeling framework that enables EO-based process-scale cost optimization with detailed water chemistry predictions (i.e., precipitation, pH, and mineral scaling). In this framework, we develop accurate water chemistry surrogate models from simulation data from OLI Systems and integrate them with the Water treatment Technoeconomic Assessment Platform (WaterTAP),[63] an open-source EO software tool for process simulation and optimization of desalination and water treatment systems. While the framework is generalizable and can be applied to numerous water treatment systems, we demonstrate our approach for hypothetical high-recovery treatment trains for brackish and seawater that includes chemical softening, pH control, standard RO, and high-pressure reverse osmosis (HPRO). We apply our framework to analyze an HPRO system since recent studies have shown it to be promising as an emerging desalination technology,[64] but there are no detailed technoeconomic assessments that predict the occurrence of mineral scaling and the necessary pretreatment to prevent it, which is especially critical for high-recovery systems. Through our analysis, we aim to provide quantitative insight that helps guide research and development for this full treatment train by comprehensively exploring the cost-optimal design across a range of water recoveries, extracting generalizable design guidelines, and performing sensitivity analyses on key performance and financial parameters. Moreover, the modeling framework presented here can be applied to evaluate and optimize other conventional and emerging applications in desalination while considering complex aqueous chemistry.

2. METHODS

We develop an EO modeling framework for process-scale cost optimization of desalination and water treatment systems with detailed water chemistry predictions. Figure 1 provides an
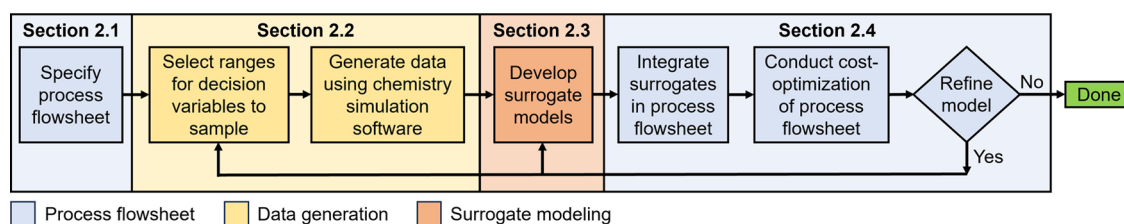
Figure 1. Overview of the generalized modeling framework.

overview of the general workflow and its relation to descriptions provided in the Methods section. Section 2.1 provides details on the feedwater composition considered and the specification of the process flowsheet. Section 2.2 describes the data-generation step to represent chemical processes, where simulations are carried out in chemistry simulation software based on specified input ranges and resolution of decision variables. Section 2.3 explains how the simulation data for chemical processes are used to develop detailed surrogate models for chemical processes. Section 2.4 focuses on process optimization and describes the integration of EO surrogate models in the process flowsheet, solving the optimization model and validating the model results against those of the chemistry simulation software. If the model results are acceptable, the workflow is complete; otherwise, depending on the diagnosis, refinement and reiteration will be required, starting again from either the data-generation or surrogate-development step (i.e., Sections 2.2 and 2.3, respectively). Section 2.5 specifies the case studies as well as the process and financial parameters that we considered in our baseline analyses.

2.1. Process Flowsheet. *2.1.1. Feedwater and Treatment Train.* We developed an optimization model to evaluate high-recovery treatment trains for brackish and seawater sources. The composition of these water sources is shown in Table 1.[65] Notably, we limit our analysis to a common subset of primary ions for the feeds. We apply our model to analyze the performance and cost of the treatment train across a wide range of recoveries (50−90% for brackish water and 50−87%

for seawater). This range exceeds the conventional range for existing systems (particularly for seawater) as we seek to investigate high-recovery systems that extend beyond typical operation and have a greater need for mineral scaling control.

To achieve such high recoveries, we consider HPRO, an emerging desalination technology that is potentially more energy-efficient than traditional evaporation-based technologies.[64,66] Conventional seawater reverse osmosis (SWRO) modules that operate at around 85 bar and commercial HPRO modules that can handle up to 120 bar are available today, but increasing maximum operating pressures would enable further increases in recovery. There is a considerable body of research focused on developing HPRO, with some recent works demonstrating that new membranes can operate at pressures in excess of 200 bar and suggesting that future advances may enable operation at even higher pressures.[64,67,68] Our analysis explores what would be achievable with the HPRO technology at such high pressures (as opposed to only what is achievable today).

Our proposed high-recovery treatment train includes chemical pretreatment and RO desalination, as shown in Figure 2. In the chemical pretreatment step, soda ash is added to soften the water by precipitating calcium carbonate and thereby reducing the calcium ion concentration.[69] Carbon dioxide is then added to lower the pH (which was increased by the addition of soda ash) and reduce the scaling tendency of carbonates.[70] Both steps allow the subsequent desalination step to recover more water before mineral scaling would occur, which we define to occur at a scaling tendency above one. In the desalination step, the water is concentrated using a single-stage process if pressure is below 85 bar and a two-stage RO process when hydraulic pressure of >85 bar is required. For our system, the second RO stage is the HPRO, with an assumed maximum operating pressure of 300 bar. The RO process includes an energy recovery device (ERD) at the end to recover any remaining energy in the retentate.

While our pretreatment processes are not typical for standard RO desalination systems, they are based on standard chemical softening for water treatment.[70−72] Typical chemical softening uses lime and/or soda ash followed by pH control via acidification. We opted to use soda ash because it can achieve high (>90%) calcium removal for both selected feedwater cases. We note that lime can be more efficient at removing calcium in the brackish water case, but for simplicity, we choose to model one chemical softening agent that is effective for both sources (Figure S1).

For acidification, we opted for carbon dioxide over other alternatives, such as hydrochloric acid and sulfuric acid, because it is self-buffering, noncorrosive, and does not require acid storage onsite.[73,74] Notably, a published industry case study cited lower costs using carbon dioxide over sulfuric acid.[74] However, we recognize that our chosen pretreatment

Table 1. Feed Composition for Brackish and Seawater Case Studies[65]

	concentrations (mg/L)	
	brackish water	seawater
Cations		
Na^+	739	10,556
K^+	9	380
Ca^{2+}	258	400
Mg^{2+}	90	1262
Anions		
Cl^-	870	18,980
SO_4^{2-}	1011	2649
HCO_3^-	385	140
TDS	3394	34,483
pH[a]	7.07	7.56
temperature (°C)	25	25

[a]The pH for each source of water is calculated using default OLI settings.
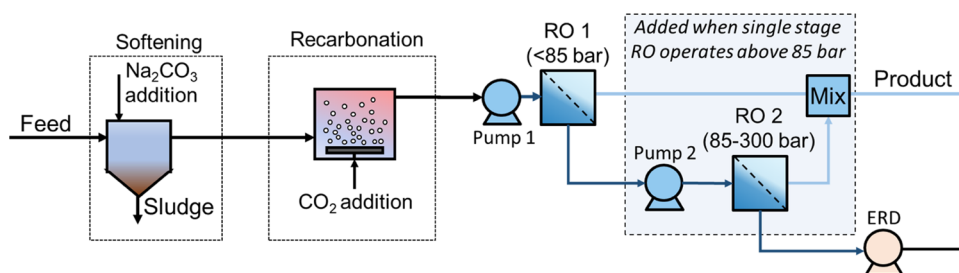
Figure 2. Schematic of the high-recovery treatment train, including chemical pretreatment via soda ash addition and recarbonation followed by RO desalination. The system enables the addition of a second high-pressure RO stage when single-stage operation exceeds 85 bar for a given water recovery. A maximum allowable pressure of 300 bar was considered for the second stage. An extended version of the figure showing how the surrogates interact with this flowsheet is shown in Supporting Information (SI) Section S4.

design is one of many options and that it is possible that other options could be better suited or more cost-effective.

We acknowledge that our pretreatment train does not use antiscalants, which is a common approach for controlling mineral scaling, and our feed compositions do not include silica, which is a primary scalant for brackish water.[75] While both are important considerations, they are out of the scope of this study. In order to incorporate antiscalants into an optimization, the model must relate the dose to its primary effect of extending the induction time, which would require considering kinetics and is fundamentally different from our proposed thermodynamic equilibrium approach (described in subsequent sections). Additionally, industry guidelines on how antiscalants can enable higher levels of supersaturation without mineral scaling are based on experimental observations and may not be applicable to the high-recovery conditions we consider.

We also exclude silica scaling and removal for two reasons. First, predicting silica scaling is challenging due to the lack of data and high-fidelity models. As opposed to other scalants considered in this work that have well-defined thermodynamic equilibrium data and models for precipitation, silica does not because it forms amorphous scales and has significant interactions with other metals. Second, silica removal is a surface complexation process via adsorption and ion exchange with magnesium hydroxide,[76,77] which fundamentally differs from the pure homogeneous precipitation mechanism demonstrated by the other scalants examined in this work. Therefore, we constrain our investigation to the ions listed in Table 1 and their precipitation-based scalants.

2.1.2. Modeling in WaterTAP. We represent the treatment train as a nonlinear programming problem with the objective of minimizing the levelized cost of water (LCOW) of the system for specified feed conditions and process and financial parameters. The LCOW is a financial metric representing the total annualized capital and operating cost normalized by water production, with units of $/m^3. The model optimizes the design and operation of the system, including the soda ash and carbon dioxide doses for pretreatment and membrane area, cross-flow velocity, and operating pressure for each RO stage.

We used the WaterTAP software package to build our optimization model. WaterTAP is an open-source Python package that supports the simulation and optimization of water treatment trains;[63,78] it is based on the IDAES Integrated Platform[79−81] and Pyomo[82,83] software packages that use EO solution strategies to provide a powerful computational capability for optimization.

We create our model by assembling the treatment train using WaterTAP's modular model library, which includes unit, property, and costing models for chemical precipitation, pumping, and RO. While additional modeling details are included in SI Section S2, a brief description of these models is as follows:

- Chemical precipitation: This unit model includes the reactions and mass balances representing (1) chemical reagent dissolution in water, (2) precipitant formation, and (3) separation of the precipitant as a sludge waste with assumed water content. In this work, we include relationships for the amount of precipitant formed and the effect of chemical pretreatment on pH by developing surrogate models from OLI simulations, as described in Sections 2.2 and 2.3.

- Pump: This unit model is a standard pump model, where the power consumption is a function of volumetric flow rate, pressure difference, and an assumed pump efficiency.

- RO: This unit model represents a one-dimensional RO stage that follows the formulation detailed in our previous work.[56,59,60] This RO model uses a continuum approach where a single stage with continuous length and width variables represents a system of discrete spiral wound RO modules. The model incorporates solution-diffusion theory to estimate water and salt flux based on the local hydraulic and osmotic pressure. The model also includes relationships for concentration polarization and pressure drop that are based on fluid flow and spacer geometry. Relevant solution properties such as density, viscosity, and osmotic pressure are determined as a function of temperature and total dissolved solids from a seawater property model based on refs 84 and 85.

- Energy recovery device (ERD): This unit is a standard turbine model used to recover remaining energy from the RO retentate stream, where the power produced is a function of volumetric flow rate, pressure difference, and an assumed turbine efficiency.

- Costs: this cost model determines the costs of the system based on the design and operating variables. It includes estimates for the direct capital and operating costs for the main equipment, as well as factors for annualizing capital costs and estimating indirect costs like auxiliary equipment, installation, and siting. The direct capital costs are based on equipment size or throughput (e.g., RO capital cost is based on the membrane area, softening capital cost is based on the kg of soda ash per day, pump capital cost is based on

power), and the direct operating costs are based on the amount of annual consumption (e.g., kWh of electricity and kg of soda ash consumed per year).

The key process and financial parameters that populate these models are shown in Table 2, which can provide additional high-level insight into the structure of the models.

Table 2. Baseline Process and Financial Parameters Used in Analyses

	value	unit	ref
Process Parameters			
soda ash softening			
solid mass fraction in sludge	20	%	98
recarbonation			
hydraulic residence time	20	minutes	70
specific energy consumption	0.11	kWh/kg-CO$_2$	99
pump			
efficiency	80	%	8
energy recovery device			
efficiency	80	%	60
reverse osmosis			
water permeability	1.51	LMH/bar	56
salt permeability	0.126	LMH	56
feed channel height	1	mm	60
feed spacer porosity	85	%	100,101
minimum observed rejection	98	%	assumed
maximum inlet velocity	0.25	m/s	assumed
standard RO maximum pressure	85	bar	56
high-pressure RO maximum pressure	300	bar	64
Financial Parameters			
soda ash softening			
equipment cost	2000	$/(kg-Na$_2CO_3$/day)	71
soda ash cost	0.19	$/kg-Na$_2CO_3$	102
recarbonation			
recarbonation basin cost	700	$/m^3 of basin	99
liquid carbon dioxide equipment cost	350	$/(kg-CO$_2$/day)	99
carbon dioxide cost	0.24	$/kg-CO$_2$	103,104
energy recovery device			
equipment cost	535	$/(m^3/h)	60
pump			
equipment cost	700	$/kW	SI Section S3
reverse osmosis			
standard RO equipment cost	30	$/m^2	56
high-pressure RO equipment cost	75	$/m^2	assumed
membrane replacement rate	20	%/year	assumed
system			
electricity cost	0.07	$/kWh	60
investment factor	2	investment cost/equipment cost	60
maintenance, labor, and chemical factor	3	% of investment cost	60
capital annualization factor	0.1	fraction of investment cost/year	60
load factor	90	%	60

2.2. Chemistry Data Generation. Detailed water chemistry and thermodynamic information are necessary to accurately predict the impact of chemical pretreatment on mineral scaling in membrane systems. In this work, we acquire detailed property information using OLI Systems.[20,86] OLI provides first-principles-based equilibrium calculations and chemistry models for electrolyte/nonelectrolyte streams and includes an extensive water chemistry database. OLI allows the computation of properties such as pH, scaling tendencies, chemical speciation, and solubility for any fully defined water stream. In this work, we used OLI Studio for exploratory and verification purposes and the OLI Engine Cloud API for programmatic calculations in our modeling workflow.

Water chemistry data for the chemical processes of interest are obtained using three steps: (1) generating relevant water compositions by sweeping across the decision variables, (2) generating the water properties through parallelized runs of isothermal flash calculations using the OLI Engine Cloud API, and (3) postprocessing the OLI output to extract the water chemistry information on interest (i.e., solid formation, pH, scaling tendency). To generate data, we used OLI's MSE thermodynamic framework, which accounts for speciation in multiphase and multicomponent systems.[19−22] The rest of this section details how we do this for pretreatment and mineral scaling.

2.2.1. Soda Ash Softening. Soda ash softening reduces calcium hardness in the feedwater by adding soda ash (i.e., sodium carbonate) and precipitating calcium carbonate. We create a soda ash softening surrogate model for each feedwater, thereby allowing the data for the surrogate to be generated by varying only the soda ash dose and keeping the feedwater composition fixed. The range and number of steps for generating the soda ash dose are shown in Table 3 for the brackish and seawater cases. For each soda ash dose, we use OLI isothermal flash calculations to determine the concentration of calcium carbonate precipitate and the resulting pH. We set the maximum value for the soda ash dose based on when the marginal addition of soda ash had a negligible impact on additional calcium carbonate formation based on OLI simulations; this occurred at around 750 and 1200 mg/L for the brackish and seawater cases, respectively (Figure S1). Solids are removed from this effluent stream with an assumed water content of 80%, with the resulting liquid stream passed to a recarbonation step.

2.2.2. Recarbonation. Recarbonation is necessary to treat the effluent from soda ash softening because the stream is saturated with calcium carbonate (i.e., scaling tendency of at least 1), and any water recovery in the desalination step will increase the scaling tendency and result in mineral scale. By adding carbon dioxide for recarbonation, the pH and calcium carbonate scaling tendency are reduced and allow subsequent water recovery. The data for the recarbonation process are generated by varying the soda ash and carbon dioxide doses for the fixed feedwater compositions. The soda ash dose is included as an input for the data generation and the surrogate model of the recarbonation process because it impacts the influent composition of the recarbonation process. This approach allows the two variables to comprehensively capture the possible water composition scenarios, as opposed to independently varying the concentrations of all of the ions, which would include more dimensions and unrealizable scenarios. The ranges and number of steps for recarbonation are shown in Table 3. The maximum carbon dioxide dose was

Table 3. Summary Model Statistics for Soda Ash and Recarbonation Surrogate Models[a]

	soda ash softening		recarbonation stage
	Brackish Water		
	OLI Simulation		
soda ash dose (min−max, no. steps)	0−750 mg/L, 76		0−750 mg/L, 76
carbon dioxide dose (min−max, no. steps)			0−300 mg/L, 60
total number of scenarios	76		4560
	Surrogate Model		
	$CaCO_3(s)$	pH	pH
model size (no. terms)	13	13	101
model training time (s)	0.07	0.08	445.74
R^2	0.9999	0.9998	0.9999
mean absolute error	0.5104 mg/L	0.0031	0.0011
maximum absolute error	7.5949 mg/L	0.0315	0.0086
	Seawater		
	OLI Simulation		
soda ash dose (min−max, no. steps)	0−1200 mg/L, 100		0−1200 mg/L, 100
carbon dioxide dose (min−max, no. steps)	NA		0−300 mg/L, 60
total number of scenarios	100		6000
	Surrogate Model		
	$CaCO_3(s)$	pH	pH
model size (no. terms)	13	13	101
model training time (s)	0.1	0.1	688.90
R^2	0.9999	0.9998	0.9997
mean absolute error	0.6626 mg/L	0.0033	0.0061
maximum absolute error	5.07 mg/L	0.0148	0.0526

[a]While the RBF models are trained on subsets of the data, all model metrics (R^2, MAE) are evaluated on the full datasets generated from OLI. Note that the number of terms for an RBF model is the number of samples plus one.

Table 4. Summary Model Statistics for Mineral Scaling Surrogate Models[a]

	$CaCO_3$	gypsum	$CaSO_4$
	Brackish Water		
	OLI Simulation		
soda ash dose (min−max, no. steps)	0−750 mg/L, 16	0−750 mg/L, 16	NA
carbon dioxide dose (min−max, no. steps)	0−300 mg/L, 16	0−300 mg/L, 16	
water recovery (min−max, no. steps)	48−94%, 24	48−94%, 24	
hydraulic pressure (min−max, no. steps)	10−110 bar, 6	10−110 bar, 6	
total number of scenarios	36,864	36,864	
	Surrogate Model		
no. training points	150	150	NA
training time (s)	8370.2	10280.6	
R^2 (0.75 < ST < 1.25)	0.96	0.99	
mean absolute error (0.75 < ST < 1.25)	0.0233	0.0082	
classification accuracy—all scenarios (%)	**99.49**	**99.85**	
	Seawater		
	OLI Simulation		
soda ash dose (min, max, no. steps)	0−1200 mg/L, 25	0−1200 mg/L, 25	0−1200 mg/L, 25
carbon dioxide dose (min, max, no. steps)	0−50 mg/L, 11	0−50 mg/L, 11	0−50 mg/L, 11
water recovery (min, max, no. steps)	48−92%, 23	48−92%, 23	48−92%, 23
hydraulic pressure (min, max, no. steps)	50−300 bar, 11	50−300 bar, 11	50−300 bar, 11
total number of scenarios	69,575	69,575	69,575
	Surrogate Model		
no. training points	150	150	150
training time (s)	12861.1	15924.5	16782.3
R^2 (0.75 < ST < 1.25)	0.97	0.93	0.88
mean absolute error (0.75 < ST < 1.25)	0.0185	0.0327	0.0425
classification accuracy—all scenarios (%)	**99.52**	**99.47**	**99.43**

[a]For the surrogate model training, the pH exiting the recarbonation stage was used as an input in place of the carbon dioxide dose. ST stands for the scaling tendency.

selected at 300 mg/L. For each generated scenario of soda ash and carbon dioxide dose, we used isothermal flash calculations in OLI to determine the outlet pH. No solid formation was observed across the simulated ranges considered in this work; therefore, the solid formation was not included in the recarbonation surrogate models.

2.2.3. Mineral Scaling. We consider mineral scaling in the desalination step by predicting the prescaling tendency of relevant solids. The scaling tendency (ST) is the thermodynamic driving force for precipitation[1] and is defined as the ratio of the ion activity product (IAP) to the solubility product (K_{sp}) with respect to a given scalant in eq 1 (alternatively referred to as or related to supersaturation ratio, scaling index, or saturation index):

$$ST = \frac{IAP}{K_{sp}} \tag{1}$$

A scaling tendency below one indicates a subsaturated solution without mineral scale formation, a value equal to one indicates a saturated solution and a value above one indicates a supersaturated solution that will lead to mineral scale formation. The scaling tendency may be computed before or after precipitation; in this work, we consider prescaling tendencies, which represent the scaling tendencies before any solids have formed.[87] Since scaling tendency can vary with temperature, as noted in Table 1, we consider a feedwater temperature of 25 °C and assume isothermal conditions throughout the full treatment train.

Within the desalination step, the maximum scaling tendency will occur where the concentrations of the scaling ions are the highest, which is at the membrane interface at the end of the last RO stage. These concentrations are dependent on two factors: (a) the extent of chemical pretreatment and (b) the operation and design of the RO stages. For our system, these two factors can be represented across four variables: (1) soda ash dose, (2) carbon dioxide dose, (3) operating pressure, and (4) water recovery rate. The ranges and the number of steps for generating the mineral scaling data are shown in Table 4. The range for the RO variables was selected to cover 50−90% water recovery (with a 2−4% buffer) and up to 100 and 300 bar for the brackish and seawater cases, respectively. For each generated scenario, we use OLI flash calculations to calculate the mineral prescaling tendencies. We also identify a list of priority mineral scalants by determining the first scalant that reached a scaling tendency of 1 as the water recovery increased from 50 to 90%.

2.3. Surrogate Models for Water Chemistry. Our modeling approach incorporates water chemistry through surrogate models, which are widely used in process systems engineering and chemical engineering.[88] This approach allows us to create an EO model that can have accurate approximations of water chemistry based on other software (i.e., OLI) and integrate it within our system model without having to implement complex semiempirical water chemistry models that are heavily dependent on hard-to-obtain data. The IDAES computational platform[80] provides a mature suite of surrogate modeling tools such as PySMO[89] and ALAMO,[90] all of which provide the algebraic representations necessary for equation-oriented optimization.[88,91,92]

A unique feature of our surrogate generation process is that the surrogates are trained directly on the decision variables rather than the ion compositions. This approach ensures that

the surrogates affect the process objective directly and allows us to reduce the dimensionality of the surrogate training problem. Further details are provided in SI Section S4.

While there are many types of surrogate models (e.g., regression, kriging, artificial neural networks), we use radial basis function (RBF) surrogate models in this work.[91] RBFs are capable of expressing highly nonlinear responses and are suitable for representing different types of complex underlying phenomena.[92] They also provide good global models for both low- and high-order nonlinear responses.[92,93]

A key decision when creating an RBF surrogate model is selecting the training points. The complexity of RBF models grows with the number of training samples, so subsampling of the training data is required to keep the model expressions at a reasonable number of terms.[92] This subsampling can be done using simple techniques like uniform grid sampling or may involve more complicated space-filling designs (e.g., Latin hypercube,[94] Hammersley sampling,[95] Centroidal Voronoi Tesselation[96]) or adaptive sampling that intermittently evaluates the surrogate against the data and selects the next point(s) based on some criteria.[97] Adaptive sampling allows us to achieve higher model accuracies than space-filling designs of the same size by strategically placing training samples where they are most needed to improve the model. Each adaptive sample is selected solely on its value added to the model's accuracy. For our RBF surrogate models, we use a simple one-shot sampling technique for soda ash softening and adaptive sampling for recarbonation and mineral scaling as follows:

- Soda ash softening: A 12-point uniform sample across its single-dimensional space (soda ash dose).

- Recarbonation: We start with an initial set of 50 Hammersley points chosen from across the two-dimensional space (soda ash and carbon dioxide dose). An adaptive sampling scheme is then employed to improve the model quality by iteratively adding the worst-predicted sample from the entire data set (i.e., the sample point with the highest deviation from the true value) to the training subset. The model is thus continuously improved by increasing training samples in the region most in need of refinement, ensuring that the model error reduces with each new training point added. Fifty points are selected with the adaptive sampling scheme.

- Mineral scaling: Given that the mineral scaling models will need to discriminate between scaling and nonscaling scenarios, in addition to regression metrics such as root-mean-square error (RMSE) and the maximum absolute error (MAE), we also consider the classification accuracy (i.e., how well the model does in predicting the occurrence of mineral scaling). We start with an initial 50 Hammersley samples across the four-dimensional space (soda ash dose, carbon dioxide dose, RO water recovery, operating pressure). Additional samples are selected adaptively in two phases. In the first phase, the new samples are selected to improve the classification accuracy. Here, adaptive sampling is conducted for 50 samples by iteratively selecting the misclassified point with the highest absolute error (i.e., when the model predicts that the scaling tendency is less than 1 when it is greater than 1 or vice versa). This improves the model's ability to classify correctly into scaling and nonscaling scenarios. In the second phase, the adaptive sampling

algorithm focuses on improving the absolute values of the model predictions around the scaling/no-scaling threshold of one. This is achieved by adaptive sampling for the points with the highest absolute error within a scaling tendency range of 0.75 and 1.25 (25% of the critical value), thus ensuring that the model is accurate within this region of interest. An additional 50 sample points are selected in the second stage. With the two-stage adaptive sampling approach, the mineral scaling surrogates achieve high classification accuracies and accurately estimate the absolute scaling tendencies between the constrained range (0.75−1.25).

Additional details on the surrogate model methodology are included in SI (S3) Section S4.

2.4. Process Optimization. For the analyses presented in this work, we solved the cost-optimization model for different conditions (e.g., different water recoveries and process and financial parameters). Each solution minimizes the LCOW by determining the optimal design and operating variables for the system (i.e., soda ash dose, carbon dioxide dose, membrane area, cross-flow velocity, and operating pressure for each RO stage) subject to the process model relationships and system constraints. One key system constraint is that the scaling tendencies of all minerals must be below one, which ensures that no mineral scaling will occur thermodynamically.

2.4.1. Surrogate Integration in Process Flowsheet. The surrogate modeling tools in IDAES allow us to easily incorporate them into the WaterTAP flowsheet. Specifically, the tools create surrogate models using Pyomo variables and constraints, which are connected to the relevant variables in the process and costing models representing the high-recovery system within WaterTAP. Figure S6 in SI Section S4 shows a schematic representation of how the generated surrogates interact with the WaterTAP HPRO flowsheet. For our system, the relevant input and output variables for each surrogate model are as follows:

1. Soda ash softening: the input is the soda ash dose; the outputs are the concentration of calcium carbonate solids and the pH of the effluent.
2. Recarbonation: the inputs are soda ash and carbon dioxide dose; the outputs are the pH in the effluent.
3. Mineral scaling: the inputs are soda ash dose, pH after recarbonation (a proxy for carbon dioxide dose), operating pressure, and water recovery; the outputs are the scaling tendencies of calcium carbonate, gypsum, and calcium sulfate.

For the mineral scaling surrogates, we add variables and constraints to the WaterTAP model to account for concentration polarization and enforce a maximum scaling tendency of 1 for all minerals. In order to incorporate concentration polarization, where the concentrations of solutes are greater at the membrane interface than in the bulk solution, we implement an equivalent water recovery that explicitly accounts for this higher concentration. This equivalent water recovery is calculated based on the predicted salt mass fraction at the membrane interface and the salt and water mass, as shown in eq 2. We determine this equivalent water recovery for every node in the membrane model, and the maximum equivalent water recovery is used as the input to the mineral scaling surrogate model, thereby ensuring the predicted scaling tendency is where the solutes are at the highest concentration. Thus, the equivalent water recovery is given by

$$X_{\text{TDS},i} = \frac{M_{\text{TDS},i}}{M_{\text{TDS},i} + M_{\text{H}_2\text{O,in}}(1 - R_{\text{eq},i})} \quad (2)$$

where $R_{\text{eq},i}$ is the equivalent water recovery, $X_{\text{TDS},i}$ is the TDS mass fraction at the membrane interface on the feed-side, $M_{\text{TDS},i}$ is the TDS bulk mass flow rate on the feed-side at node i, and $M_{\text{H}_2\text{O,in}}$ is the mass flow rate of water into the desalination system.

2.4.2. Solving the Model. We use the default open-source IPOPT with the MA27 linear solver in WaterTAP. While it is a local solver, we find that the solutions exhibit smooth trends in the variables and are not dependent on the initial guess, thereby suggesting that the local solver is performing well. The LCOW minimization problem contains 1901 and 3498 variables and 1896 and 3490 constraints for single- and two-stage RO systems, respectively. These systems can be distilled to 5 and 8 decision variables (i.e., the operating pressure, membrane area, and cross-flow velocity for each stage, in addition to the soda ash and carbon dioxide doses) for the single- and two-stage RO problems, respectively.

2.4.3. Validation of Results. Once we obtain an optimal solution, we perform a set of validation checks to ensure the accuracy and reliability of our solutions. First, we verify that the optimal solutions are not constrained by our surrogates by checking that the optimal values of the decision variables do not fall at the bounds of the variable ranges. If a decision variable is at the bounds, it indicates that the decision space was constrained too tightly, and we need to return to the data-generation step and expand the variable range. We also employ a multistart approach, ensuring that different initial guesses for the decision variables do not result in different solutions. Finally, to ensure the validity and accuracy of the results, we compare the predictions of the surrogate models with the true OLI values for the optimal values of the decision variables, ensuring that the surrogate prediction error is within an acceptable limit. Large differences between the OLI and surrogate predictions indicate that the surrogate does not capture the underlying phenomena to a fine enough resolution, requiring us to revisit the data-generation and surrogate-development steps.

2.5. Case Study Parameters. For the purpose of discussion, we highlight three water recovery rates for each source that result in similar design and operation based on the degree of softening (i.e., no, low, and high softening requirements). For brackish water, water recoveries of 50, 70, and 90% correspond to cases 1, 2, and 3, respectively. For seawater, water recoveries of 50, 75, and 85% correspond to cases 4, 5, and 6, respectively.

Table 2 presents the base process and financial parameters for our analysis. These parameters populate the unit and costing models that are described briefly in Section 2.1.2. Notably, we constrain the minimum observed rejection of TDS at 98%, preventing the occurrence of an impractical operating regime where rejection would be decreased to counteract the effects of concentration polarization. For the same reason, we also set the maximum inlet cross-flow velocity of RO to 25 cm/s. Since our work is focused on optimizing the treatment train, we did not consider the costs of sourcing the feedwater, disposing the residual solids and brine, or distributing the product water. While including these additional activities would add to the overall LCOW, it is expected that their inclusion would not impact our optimized treatment train
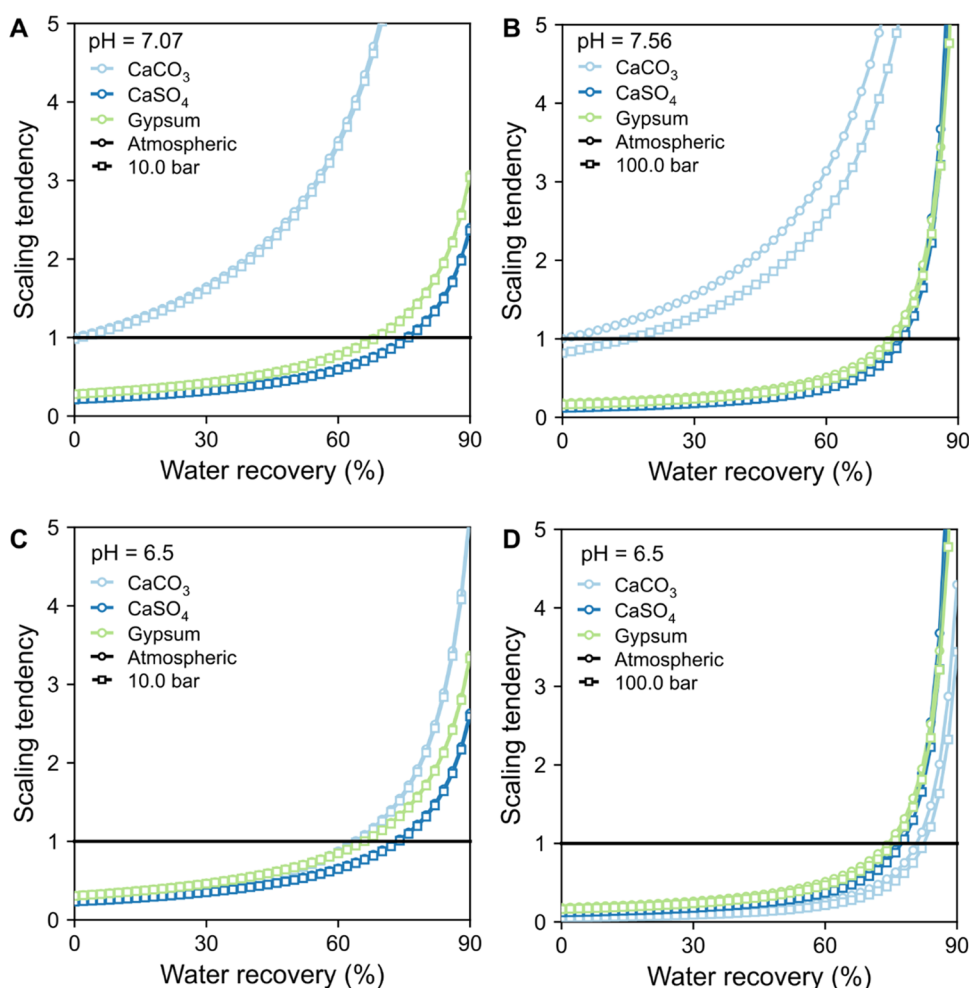
Figure 3. Primary mineral prescaling tendencies as a function of equivalent water recovery for each water source and two pH scenarios and hydraulic pressures. The brackish and seawater sources are shown on the left (A, C) and right (B, D), respectively. Plots (A) and (B) are at the unadjusted pH values estimated by OLI, which are 7.07 and 7.56 for the brackish and seawater cases, respectively. Plots (C) and (D) are at an adjusted pH of 6.5. For both cases, the pH was dropped to 6.5 through the addition of carbon dioxide (C and D). Within each plot, markers are used to note two hydraulic pressures, including atmospheric and higher pressures (10 bar for brackish water and 100 bar for seawater).

design and operation because the amounts of feedwater, waste solids, waste brine, and product water are closely tied to the specified recovery and are essentially fixed costs (i.e., the modeled decision variables do not impact them). Additionally, membrane water and salt permeability coefficients for brackish and seawater cases were conservatively assumed to be the same to facilitate direct comparison; however, sensitivity analyses shown later in Section 3.3.3 show the effects of varying these parameters on LCOW. More details on the selected process and financial parameters are provided in SI Section S3.

3. RESULTS AND DISCUSSION

We use OLI water chemistry predictions and our optimization model to explore the cost-optimal design of the high-recovery treatment trains for brackish and seawater treatment. Section 3.1 presents mineral scaling tendencies calculated via OLI for the brackish and seawater source compositions shown in Table 1. Section 3.2 describes the surrogate models developed for soda ash dose, carbon dioxide dose, mineral scaling tendency, and assessment of the fits to the underlying data. Section 3.3 presents cost-optimization results for the case studies, cost-optimal design results over a range of recovery rates, and sensitivity analyses with respect to key process and financial

parameters. Additionally, supporting data for the figures are provided in the SI.

3.1. Mineral Scaling for Selected Water Sources. Using OLI, we determine calcium carbonate $(CaCO_3)$ and gypsum $(CaSO_4.2H_2O)$ as the primary scalants for both brackish and seawater, as well as calcium sulfate anhydrite $(CaSO_4)$ for seawater. This list of scalants is in agreement with sparingly soluble salts reported in the literature.[2,3,105,106] In general, the scaling tendencies for these minerals increase with increasing water recovery, decrease with decreasing pH, and decrease with increasing hydraulic pressure (Figure 3). The scaling tendency of calcium carbonate is strongly affected by pH, while hydraulic pressure has a noticeable effect only at high pressures (e.g., 100 bar). The scaling tendencies of calcium sulfate anhydrite and gypsum are minorly affected by both the hydraulic pressure and pH.

We observe that the brackish and seawater feeds are supersaturated with calcium carbonate (i.e., scaling tendency above 1) at the pH values calculated by OLI and would thermodynamically precipitate out in the softening step and before desalination (Figure S1). After the initial precipitation to saturation (i.e., scaling tendency equals 1), we find that scaling tendencies increase with water recovery (Figure 3A,B).
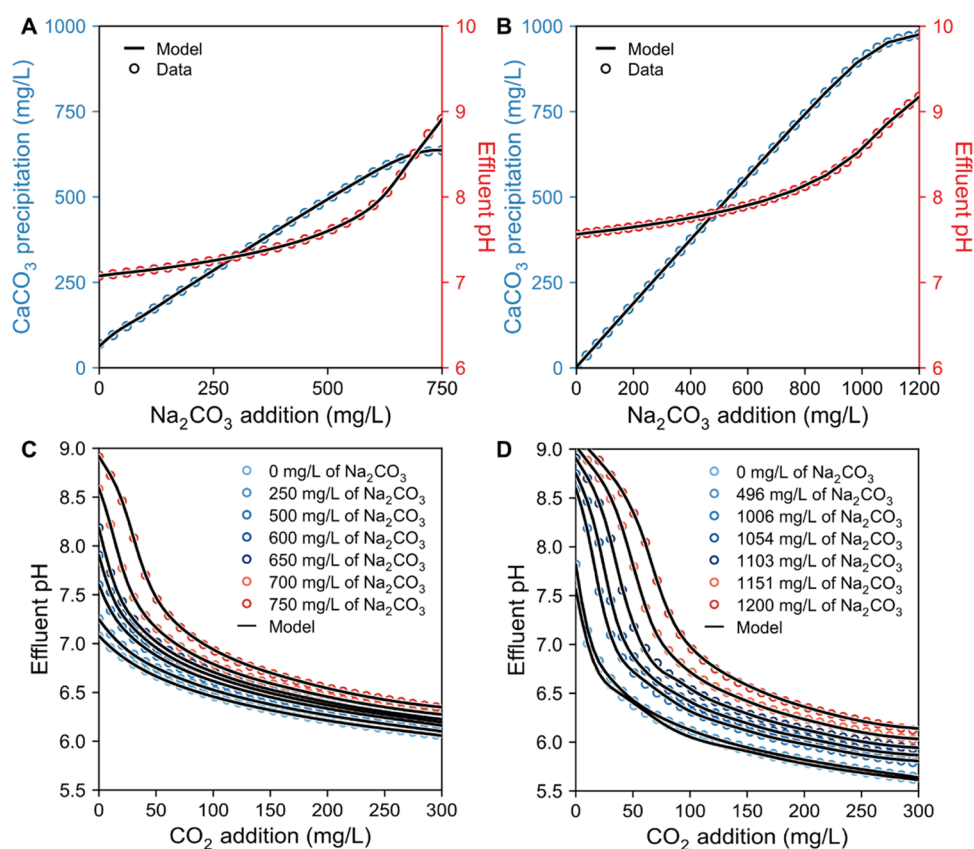
Figure 4. Calcium carbonate concentration and pH as functions of soda ash dosing are shown for brackish (A) and seawater (B) sources. Effluent pH values at the outlet of the recarbonation stage as a function of carbon dioxide addition are shown for a range of soda ash doses in the brackish (C) and seawater (D) sources. Training data and surrogate model predictions are represented by points and lines, respectively.

This finding emphasizes that, at a minimum, some pH adjustment is necessary for these water sources to operate the desalination process below a scaling tendency of 1. Our analysis also reveals that once the pH has been sufficiently lowered to prevent calcium carbonate scaling (maximum scaling tendency equal to 1), the next likely scalant of concern is gypsum. The scaling tendencies of calcium sulfate anhydrite and gypsum cannot be significantly reduced with pH and hydraulic pressure, thereby requiring more extensive pretreatment (i.e., calcium removal through soda ash softening) to achieve increased recovery rates.

3.2. Surrogate Models for Pretreatment and Mineral Scaling Prediction. As described in Sections 2.2 and 2.3, we create surrogate models based on OLI simulated data for (1) soda ash softening, (2) recarbonation, and (3) mineral scaling within the RO process. Figure 4 and Table 3 present the OLI simulation data and surrogate model details and statistics for soda ash softening and recarbonation, while Table 4 presents the surrogate model details and statistics for mineral scaling.

The soda ash softening surrogate model predicts the calcium carbonate precipitation (milligrams per liter) and outlet pH as a function of soda ash dose. The 13-term RBF surrogate model accurately represents the OLI simulation data and captures the curvilinear relationship between the input and outputs, with R^2 > 0.99 and mean absolute errors below 1 mg/L for calcium carbonate precipitation and 0.004 for pH in both water sources.

The recarbonation surrogate models predict the effluent pH as a function of the carbon dioxide dose and upstream soda ash dose. The 101-term RBF surrogate models with adaptive

sampling accurately capture the underlying phenomena with R^2 > 0.999 and mean absolute errors of 0.001 and 0.006 for the pH of brackish and seawater, respectively. The adaptive sampling models outperform surrogates with the same number of terms generated using space-filling (one-shot) sampling methods, albeit at the expense of computational time (i.e., hundreds of seconds compared to seconds). Additional details are included in SI Section S4.

The mineral scaling surrogate models predict the scaling tendency of the relevant minerals as a function of four variables: soda ash dose, recarbonation effluent pH (directly related to the carbon dioxide dose), water recovery, and hydraulic pressure. These 151-term RBF surrogate models with adaptive sampling have classification accuracies greater than 99.4% (classifying whether the scaling tendency is correctly predicted to be greater than or less than 1) across all three mineral scalants and the two water sources. Between scaling tendencies of 0.75 and 1.25, which we considered as the region of interest for sensitivity analyses (see Section 3.3.4), the surrogate models have an R^2 > 0.88 and a mean absolute error of less than 0.05. While our resulting models are sufficiently accurate, we found that it was challenging to develop surrogates for this large and highly nonlinear data set. Our adaptive sampling approach that first prioritizes classification errors and then errors within the region of interest performed significantly better than one-shot sampling and regression models, with additional details shown in SI Section S4.

During the development of this work, we evaluated several sampling and surrogate modeling approaches. We found that adaptive sampling performs better than one-shot sampling for

Table 5. Summary of Cost-Optimal Results for Brackish and Seawater Case Studies at Three Different Recovery Rates (Low, Medium, and High)

	brackish water			seawater		
	case 1	case 2	case 3	case 4	case 5	case 6
Case Conditions						
water recovery (%)	50	70	90	50	75	85
System Metrics						
final brine concentration (g/L)	6.79	11.6	37.2	69.8	141	240
final permeate concentration (g/L)	0.04	0.07	0.08	0.40	0.65	0.70
pretreatment calcium removal (%)	9.64	19.70	75.6	0.26	4.13	68.0
solids generation (mg/L of feed)	62.1	127	487	2.61	41.2	679
pH after soda ash addition	7.07	7.12	7.58	7.56	7.58	8.04
pH after recarbonation	6.57	6.35	6.20	7.13	6.67	6.70
SEC (kWh/m^3)	0.88	0.72	1.28	2.85	3.40	4.45
Decision Variable						
soda ash dose (mg/L)	0.00	63.2	492.3	0.00	41.3	729
carbon dioxide dose (mg/L)	71.2	145	275	7.70	22.6	30.0
stage 1 membrane area (m^2)	92.3	185	106	91.7	90.7	100.5
stage 1 inlet hydraulic pressure (bar)	18.7	17.6	35.4	60.9	77.6	85.0
stage 1 inlet cross-flow velocity (m/s)	0.20	0.25	0.25	0.19	0.20	0.21
stage 2 membrane area (m^2)					53.3	39.7
stage 2 inlet hydraulic pressure (bar)					113.1	219.8
stage 2 inlet cross-flow velocity (m/s)					0.25	0.25
Financial Metrics						
levelized cost of water ($/m^3)	0.31	0.49	1.32	0.43	0.61	2.10
capital ($/m^3)	0.12	0.24	0.79	0.14	0.22	1.21
operating ($/m^3)	0.20	0.25	0.53	0.28	0.39	0.90
soda ash softening ($/m^3)	0.00	0.16	0.97	0.00	0.10	1.52
recarbonation ($/m^3)	0.09	0.12	0.17	0.02	0.03	0.03
pumps ($/m^3)	0.11	0.08	0.12	0.30	0.33	0.43
membrane ($/m^3)	0.09	0.13	0.06	0.09	0.15	0.11
energy recovery devices ($/m^3)	0.02	0.01	0.00	0.02	0.01	0.00
Mineral Scaling Tendency						
calcium carbonate	1.00	1.00	1.00	1.00	1.00	1.00
gypsum	0.73	1.00	1.00	0.41	1.00	1.00
calcium sulfate anhydrite				0.34	0.84	0.94

this problem, and cubic RBF models generally outperform other surrogate modeling techniques (such as regression models). Besides resulting in better statistical metrics (i.e., R^2, mean absolute error, maximum absolute error, and classification accuracy), the RBF surrogates with adaptive sampling have significantly better behavior when used in the optimization model than those with one-shot sampling. Specifically, one-shot sampling RBFs and nonlinear regression models frequently result in poor, local solutions, meaning that their relationships are not smooth for key dimensions throughout the space. We have verified that our presented surrogates do not produce local minima by solving with high granularity across a range of water recoveries and ensuring that initial guesses for the decision variables do not result in different solutions.

3.3. Cost Optimization with Mineral Scaling Prediction. *3.3.1. Cost-Optimal Design for Brackish and Seawater Cases.* We use our WaterTAP model with detailed water chemistry surrogate models to minimize the LCOW for the brackish and seawater treatment trains. For any specified water recovery, the model determines the cost-optimal values for the primary decision variables, including the soda ash dose and carbon dioxide dose for pretreatment, as well as the operating pressure, membrane area, and inlet cross-flow velocity for each RO stage. We explore cost-optimal designs

for each water source at three water recovery rates (low, medium, and high recovery) for a total of six cases, as presented in Table 5. As described in Section 2.5, the six cases also represent three levels of pretreatment: (1) cases 1 and 4 with low recovery have no softening and only require recarbonation as pretreatment, (2) cases 2 and 5 with medium recovery require recarbonation and low softening, and (3) cases 3 and 6 with high recovery require recarbonation and significant softening.

Table 5 presents the cost-optimal results for the six cases. The LCOW ranges between $0.31− $1.32 and $ 0.43−$2.10/ m^3 for the brackish and seawater sources, respectively. While costs increase with increased water recovery, most of the increase for high-recovery cases is attributed to soda ash softening. For the highest recovery cases (i.e., cases 3 and 6), soda ash softening comprises 70−75% of the LCOW. For the lowest recovery cases, the soda ash softening cost is zero because softening is unnecessary at these low recoveries to prevent mineral scaling. Recarbonation costs also increase with water recovery, albeit at a lower rate than soda ash softening. The recarbonation costs increase with water recovery because additional carbon dioxide dosing is necessary to further reduce the pH and prevent the scaling tendency of calcium carbonate from exceeding 1. For the seawater source, the pump costs increase with water recovery because higher operating
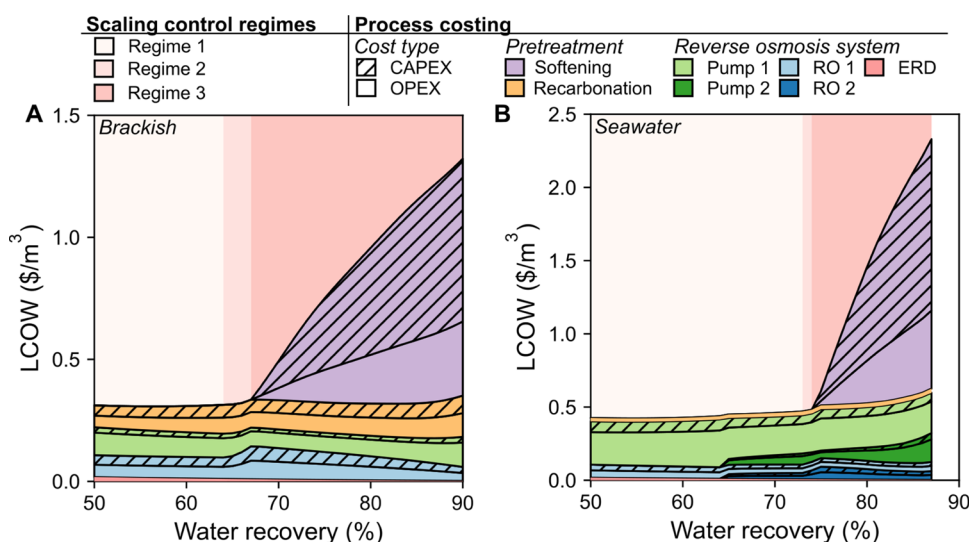
Figure 5. Breakdown of optimal LCOW categorized by components for the brackish (A) and seawater (B) cases. For seawater, the cost profile ends at 88% recovery because pressures higher than 300 bar, the maximum pressure considered in this work, are required. Regimes 1, 2, and 3 denote ranges of recovery rates where scaling is controlled by a particular mechanism. Regime 1: calcium carbonate scaling control governed by recarbonation; Regime 2: calcium carbonate and gypsum scaling control governed by adjustment in RO design and operation; Regime 3: calcium carbonate and gypsum scaling are controlled by all decision variables, including soda ash addition.

pressures are required to overcome the higher osmotic pressures of the brine. However, for the brackish water source, there is not a consistent trend in pump costs due to complex trade-offs associated with marginal operating and capital costs for the pumps, membranes, and pretreatment. Similarly, there is no consistent trend in membrane costs for both water sources. In short, there are trade-offs between pretreatment and the RO system (pumps and membranes) attributed to balancing the extent of concentration polarization, which dictates scaling tendency at the membrane interface. These trade-offs are explained in more detail in Section 3.3.2.

There are three notable differences between the optimal treatment train design and operation for the brackish and seawater sources. First, none of the brackish water cases require a second high-pressure RO stage; all of their desalination targets can be achieved with a standard RO stage requiring less than 36 bar of hydraulic pressure across all recoveries. On the other hand, only the low-recovery seawater case can be achieved with standard RO (less than 85 bar), while the medium- and high-recovery seawater cases require a high-pressure RO stage to overcome the brine osmotic pressure. For these two-stage designs, we find that the cost-optimal membrane area for the second stage is lower than that for the first stage. This result is expected because the high-pressure RO stage treats a smaller volume of water and is modeled with a higher cost than the standard RO stage (i.e., $75/m^2$ vs $30/m^2$). Second, since the seawater cases are operated at significantly higher pressures than the brackish water cases, there is a substantial difference in the components that make up the RO system costs (including pump and membrane costs). For the seawater cases, the pump costs (including capital and operating costs) make up 70−80% of the RO system costs, while for the brackish water cases, they only make up 40−60%. Third, the brackish water cases have significantly higher recarbonation costs than the seawater cases ($0.09−0.17/m^3$ compared to $0.02−0.03/m^3$). This occurs because the brackish water source considered in this work has a higher buffer capacity, attributed to the higher concentration

of bicarbonate,[107] when compared with the composition of the seawater source (see Table 1); bicarbonate concentration in brackish water exceeds that of seawater by a factor of 2.75. Thus, the brackish source has a higher resistance to a change in pH as carbon dioxide is added to the solution. Consequently, the cost-optimal carbon dioxide dose required for brackish water cases can be more than 9 times greater than that for seawater cases.

Table 5 also presents the maximum scaling tendency for each mineral in the treatment train. These scaling tendencies provide insight into which minerals are influencing pretreatment. If the scaling tendency is 1, then the maximum allowable scaling tendency constraint is active, and some pretreatment action is necessary to ensure that it does not exceed 1. For the low-recovery cases, only calcium carbonate has a scaling tendency of 1 and influences the carbon dioxide dose. For the medium- and high-recovery cases, both calcium carbonate and gypsum have scaling tendencies of 1 and influence the soda ash and carbon dioxide dose. For all of the cases, calcium sulfate anhydrite does not reach a scaling tendency of 1 and does not directly influence pretreatment. This is in agreement with the literature, which indicates that while calcium sulfate anhydrite forms more readily at elevated temperatures (e.g., ≥40 °C), gypsum is the dominant form of calcium sulfate at 25 °C,[12] the temperature considered in this work. In addition to the model statistics summarized in Table 4, for each of the six cases, we assessed the accuracy of our mineral scaling surrogate predictions by comparing the scaling tendencies obtained from the surrogates for our optimal solutions with those of OLI simulations with the same soda ash dose, carbon dioxide dose, equivalent water recovery, and hydraulic pressure. We found that our error in the region of interest (between 0.75 and 1.25) was satisfactorily low at less than 5% (Table S3). As expected, the largest errors occurred for low scaling tendencies outside the region of interest, where we explicitly did not prioritize accuracy, because low scaling tendencies do not influence the pretreatment decision variables and do not impact the optimal solution in our model.
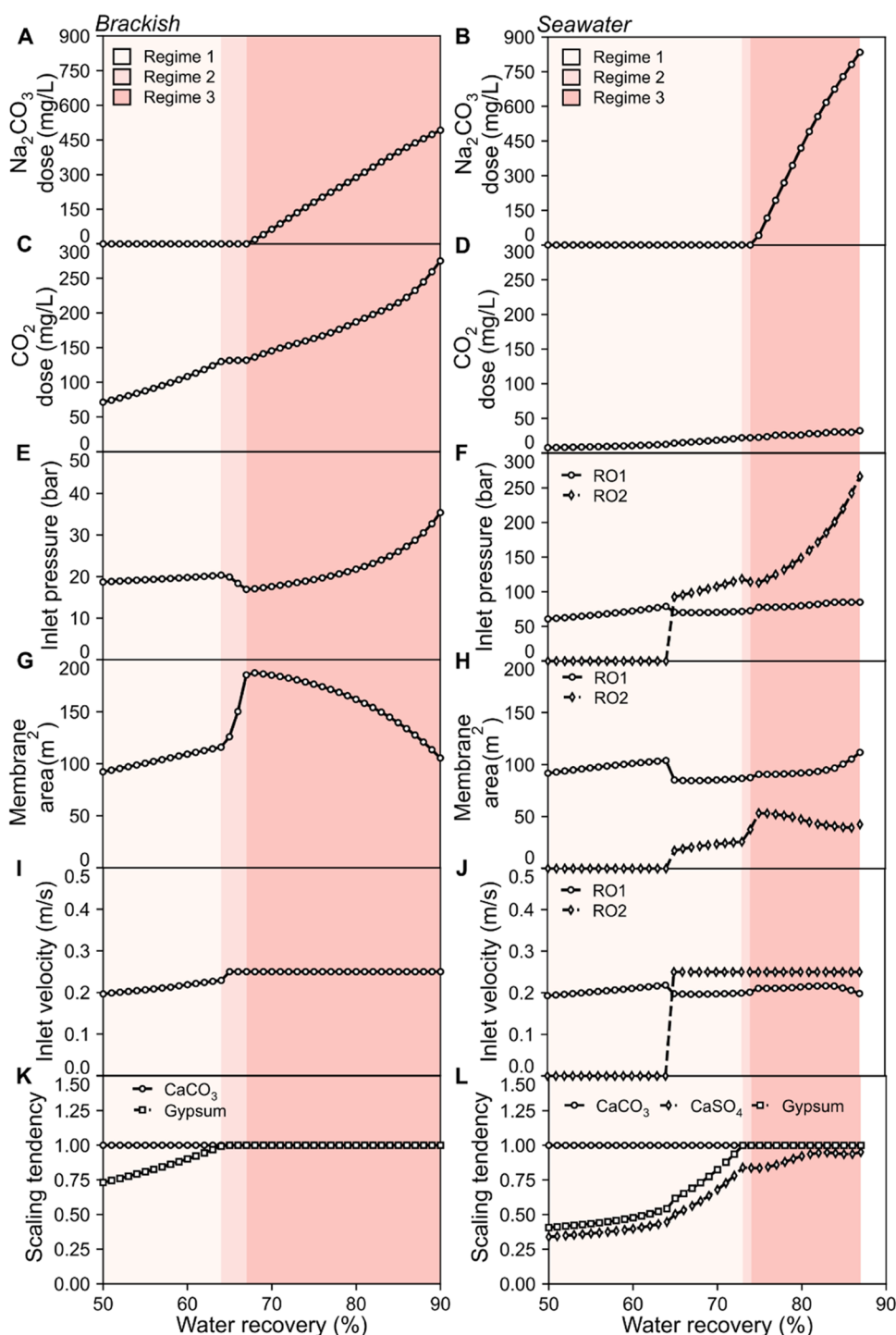
Figure 6. Cost-optimal decision variables are shown for recovery rates from 50−90% and 50−88% for brackish (left column) and seawater (right column), respectively. Decision variables include soda ash (Na_2CO_3) dose (A, B), carbon dioxide (CO_2) dose (C, D), RO inlet pressure (E, F), RO membrane area (G, H), RO inlet velocity (I, J), and scaling tendency (K, L). Regimes 1, 2, and 3 denote ranges of recovery rates where scaling is controlled by a particular mechanism. Regime 1: calcium carbonate scaling control governed by recarbonation; Regime 2: calcium carbonate and gypsum scaling control governed by adjustment in RO design and operation; Regime 3: calcium carbonate and gypsum scaling control are influenced by all decision variables, including soda ash addition.

3.3.2. Cost-Optimal Design across Water Recoveries. To further investigate the effect of recovery rate on cost-optimal design, we apply our cost-optimization model from 50 to 90% recovery for brackish and seawater sources. We find that there are three regimes that describe the cost-optimal design and operation. These three regimes can be characterized by which decision variables primarily control mineral scaling. In the first regime, which occurs at lower water recoveries, carbon dioxide dosing primarily controls calcium carbonate mineral scaling. In the second regime, which occurs for a narrow recovery window, both calcium carbonate and gypsum mineral scaling occur, and these are controlled via changes to the RO design and operation. In the third regime, which occurs for higher water recoveries, all decision variables, including soda ash dose,

control calcium carbonate and gypsum mineral scaling. These regimes are noted in Figures 5 and 6, which show the optimal LCOW breakdown and decision variables across the full range of recovery rates, respectively. For brackish water, regimes 1, 2, and 3 correspond to 50−64, 64−67, and 67−90% recovery, respectively. For seawater, regimes 1, 2, and 3 correspond to 50−73, 73−74, and 74−88% recovery, respectively.

In the first regime, we find that the cost-optimal LCOW increases by a relatively small amount with increasing water recovery, even though the optimal process design and operation change continuously. The LCOW increases by only 0.2% for the brackish water source from 50 to 63% water recovery and by 10.4% for the seawater source from 50 to 72% water recovery (Figure 5). Throughout this regime, the cost-optimal carbon dioxide dose, operating pressure, membrane area, and inlet cross-flow velocity increase with water recovery (Figure 6). While these changes increase the overall capital and operating costs, they do not significantly change the LCOW because of the increased water production. We find that these optimal solutions balance trade-offs between the pretreatment and the RO system by balancing water flux and the extent of concentration polarization. While higher water flux reduces the necessary membrane area and its associated costs, it requires higher operating pressures and higher carbon dioxide dosing because the increased concentration polarization requires greater control of mineral scaling. SI Section S5 provides additional variables (e.g., water flux and specific energy consumption) that can provide insight into the optimal design.

Across the second regime, the LCOW modestly increases by 6.6 and 2.2% in the narrow water recovery range for the brackish and seawater cases, respectively. This second regime is different from the first regime in three ways: (1) the gypsum scaling tendency is predicted to be one and must be controlled, (2) the optimal carbon dioxide dose stops increasing with water recovery, and (3) the optimal RO system design and operation dramatically change. All three differences are directly related to how the system design and operation change to control gypsum scaling. Since the scaling tendency of gypsum is minorly impacted by pH, there is no increase in carbon dioxide dose; instead, the RO system design and operation shift to reduce maximum ion concentrations. The RO system is operated with lower pressures, higher membrane areas, and higher inlet cross-flow velocity to reduce water flux and concentration polarization (Figure 6). We find that concentration polarization is minimized at the end of this regime, and the solutions are constrained by the maximum allowable inlet cross-flow velocity (25 cm/s) and minimum allowable salt rejection (98%), as shown in Table 2. This result suggests that the cost increase associated with minimizing concentration polarization in RO through more membrane area and higher pressure drop is cheaper than soda ash softening, which is the alternative approach to control gypsum scaling. However, there are limitations to shifting RO system operation, with this approach only feasible over a relatively narrow range of recoveries (4 and 2% range for brackish and seawater, respectively). Eventually, soda ash softening becomes the only avenue for increased recovery.

In the third regime, soda ash softening is used to precipitate calcium and control gypsum scaling. The LCOW increases dramatically by factors as high as 3.4 and 3.8 for brackish and seawater sources, respectively. As described previously, most of this cost increase is due to soda ash softening, constituting over 70% of the LCOW in both water cases at high recovery, with

the capital cost being the primary component. Note that the softening capital cost increases with soda ash dose because larger equipment is necessary for the higher throughput. Thus, our assumed capital cost parameter for softening, $2000/kg of soda ash per day, plays a significant role in the predicted LCOW of the treatment train. A brief literature review shows that there is high uncertainty in this capital cost parameter value.[71,108,109] Later, in Section 3.3.3, we conduct a sensitivity analysis to account for this uncertainty in the LCOW. Furthermore, while only soda ash softening was considered in this analysis, lime addition can offer higher efficiency in removing calcium, reduce acid addition under certain conditions, and potentially result in reduced costs when lime or a mixture of lime and soda ash is used (Figure S1).

The regime has expected trends in optimal decision variables, with the soda ash dose, carbon dioxide dose, and RO operating pressure all increasing with water recovery. We find that the optimal inlet cross-flow velocity for the final RO stage is at the maximum allowable value, demonstrating that concentration polarization is being minimized. A counter-intuitive finding is that the membrane area generally decreases with water recovery in this regime. However, this trend is expected when considering our modeling constraints. By the end of the second regime, the RO system design and operation is already minimizing concentration polarization to the largest extent possible by having low water flux at the end node, subject to a constraint on minimum allowable rejection (SI Section S5). In the third regime, there is no remaining flexibility for rejection to decrease. Therefore, as water recovery increases, hydraulic pressure must increase to overcome the increasing brine osmotic pressure and to ensure that the constraint for minimum allowable rejection is satisfied; higher concentrations require higher average water flux to offset the increased salt flux. Another complicating factor is that we only consider one- and two-stage systems, which, for the seawater case, results in designs with significant declines in permeate flux from the inlet and outlet of the stage.

The results obtained here clearly show the benefits of both pretreatment and the HPRO technology. Traditional SWRO systems typically operate at recovery rates of up to ≈50%.[110] By incorporating pretreatment into these systems and using HPRO modules available today (up to 120 bar),[64] the treatment train can be operated at recovery rates of up to about 76%. The results suggest that through pH adjustment and minor operational modifications, existing RO systems could realize an increase in recovery of more than 45% (50−74%) with only a 14% increase in costs. The recent developments in membrane design that allow for operation at pressures up to 200 bar[68] enable recovery rates up to 83%. Our analysis further suggests that water recovery rates of up to 87% are possible for seawater below our limit of 300 bar. However, such systems will have significant costs due to the extensive pretreatment required to operate at such high recoveries.

Overall, our cost-optimization approach enables us to conduct a detailed technoeconomic assessment for high-recovery treatment trains while accounting for pretreatment and mineral scaling. In practice, water treatment engineers can complete analyses like these but often with manual adjustment of the decision variables and using disjointed modeling platforms (e.g., one for mineral scale prediction, one for RO modeling, and one for costing). Each case study would take time-consuming iterations and make it impractical to create
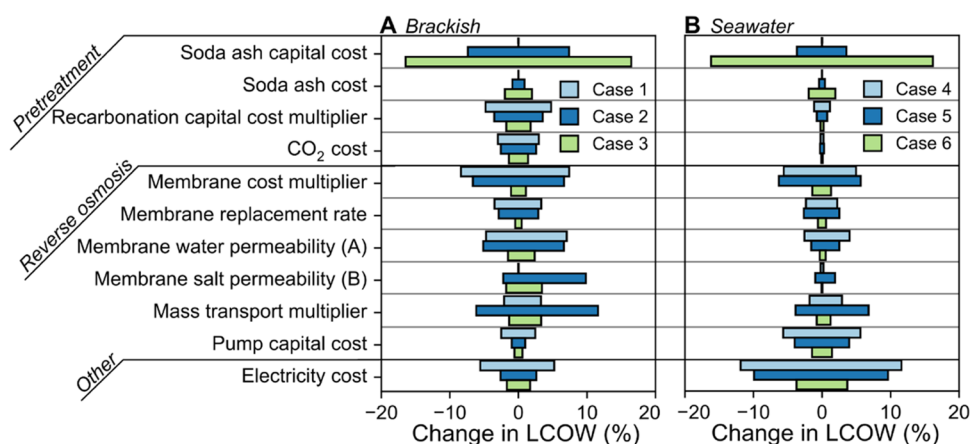
Figure 7. Tornado plot showing LCOW sensitivity to a range of financial and process variables presented in Table 2 for brackish (A) and seawater (B) cases. The results were obtained by varying the base value of each parameter by ±25%. Cases 1, 2, and 3 correspond to brackish water cases with recovery rates of 50, 70, and 90%, respectively. Cases 4, 5, and 6 correspond to seawater cases with recovery rates of 50, 75, and 85%, respectively.

analyses that have a high number of cases, as shown in Figures 5 and 6. However, these obstacles can be overcome once an optimization model is developed in a centralized modeling platform such as WaterTAP. Additionally, the optimization model can be readily extended for further analyses, such as the sensitivity analyses presented in the next section.

3.3.3. LCOW Sensitivity to Changes in Process and Financial Parameters. For the six case studies, we perform sensitivity analyses on the select process and financial parameters from Table 2 by independently varying them by ±25% and quantifying their impact on the LCOW (Figure 7). In addition to parameters from Table 2, we also group some parameters into multipliers as follows: (1) membrane capital cost multiplier for both the standard and high-pressure stages, (2) recarbonation capital cost multiplier for both the recarbonation basin and liquid carbon dioxide equipment, and (3) mass transport multiplier, which modifies the relationship calculating the mass transfer coefficient. These sensitivity analyses are intended to capture the impact of uncertainty in our parameters, as well as project potential changes in LCOW due to advancement in process performance or changes in component costs. Additionally, for all sensitivity results, all decision variables are reoptimized for each solution, thereby capturing the shift in cost-optimal design and operation as the process and financial parameters change.

In both water sources, pretreatment capital costs have a larger effect on LCOW than on raw chemical costs. The LCOW varies by up to ±16.5% for the high-recovery cases (i.e., cases 3 and 6) when we vary the capital cost of the soda ash dosing system but only varies by ±1.9% when we vary the cost of soda ash. Overall, the capital cost of the soda ash dosing system has the most significant effect on LCOW at high recovery (cases 3 and 6), indicating that substantially reducing this capital cost or identifying less costly pretreatment alternatives would be key for enabling cost-effective, high-recovery systems. Similarly, the LCOW varies by up to ±4.8% for changes in the recarbonation capital cost multiplier and only ±3.0% for changes in carbon dioxide cost for the brackish water cases. Seawater cases have significantly less sensitivity to recarbonation costs than brackish water cases because the carbon dioxide dosage is an order of magnitude lower for seawater. Overall, while the LCOW may be sensitive to

changes in capital cost for pretreatment, changes in chemical costs do not weigh as significantly on the overall LCOW. Thus, while the market (and by extension, price) for carbon dioxide can be unstable,[103,104] our sensitivity analysis of the LCOW indicates that those instabilities will have minimal influence on the overall LCOW of the water treatment train.

The LCOW is most sensitive to changes in the RO parameters when the soda ash dosing is minimal. The membrane capital cost multiplier has one of the largest effects on the LCOW, with a reduction of up to 8.4% for the low and medium recovery cases (cases 1, 2, 4, and 5). The mass transport multiplier has the highest effect on the LCOW for the medium recovery cases (cases 2 and 5). These cases are particularly sensitive to changes in the mass transfer coefficient because they are closest to regime 2, where the soda ash dose can be reduced significantly by minimizing concentration polarization. The membrane transport properties (water and salt permeability coefficients) have a low or moderate effect on the LCOW, with the water permeability generally having a greater effect. We also find that degradation in membrane properties increases LCOW more than the respective improvements decrease LCOW. For example, an increase in water permeability by 25% reduces LCOW by 4.7 and 2.6% for brackish case 2 and seawater case 4, but a decrease in water permeability by the same amount increases LCOW by 7.0 and 4.0%, respectively.

The LCOW sensitivity to electricity and pump costs shows clear trends. For both water sources, the electricity and pump costs have the greatest effect on LCOW for the lowest recovery cases. As the water recovery increases, the fraction of costs from the RO system, including electricity use and the pumps, decreases and has less impact. As expected, we find that the seawater cases are more sensitive to electricity and pump costs because they operate at higher pressures and specific energy consumption.

3.3.4. LCOW Sensitivity to Changes in Maximum Scaling Tendency. In this work, we consistently assumed that the scaling tendency could not exceed 1. While this is the point where mineral scaling would occur at equilibrium, in practice, heterogeneous nucleation can affect whether scale will form at a given scaling tendency. Furthermore, nucleation can be regarded as a stochastic process.[35,36,111,112] Thus, we present a
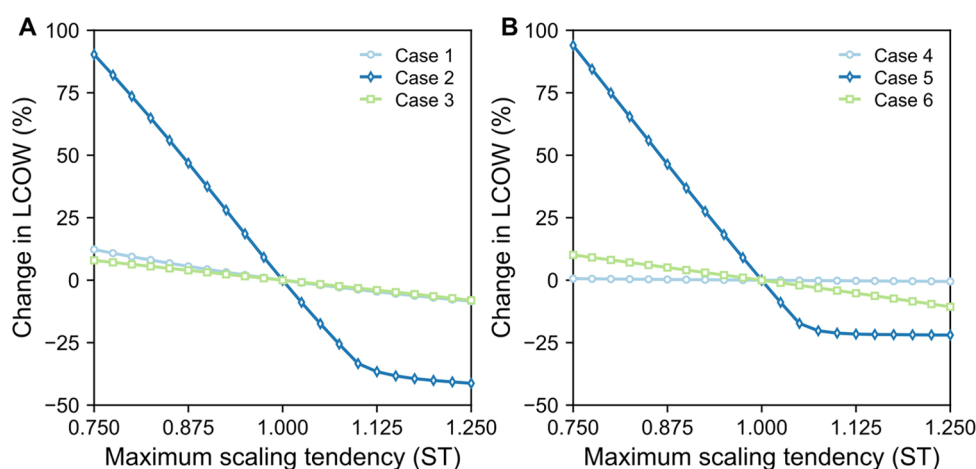
Figure 8. Effect of maximum scaling tendency on percent change in LCOW, with respect to a baseline maximum scaling tendency of 1, for brackish (A) and seawater (B) cases.

sensitivity to the maximum allowable scaling tendency and its impact on the LCOW in Figure 8.

We find that varying the maximum scaling tendency has a wide range of impacts on the LCOW across the cases. For some cases (cases 2 and 5), the LCOW can vary dramatically, whereas for other cases (case 4), there is little to no effect on LCOW. Cases 2 and 5 are impacted greatly because changing the maximum scaling tendency shifts in which regime they operate in. When the maximum scaling tendency is increased above ~1.1, both cases 2 and 5 no longer use soda ash to control gypsum scaling, thereby reducing costs by 41 and 22% for the brackish and seawater cases, respectively. Further increases in the maximum scaling tendency for these cases produce minimal cost reductions. When the maximum scaling tendency is decreased to 0.75, cases 2 and 5 require significantly more soda ash dosing, increasing costs by more than 85% for both cases. We do not observe these large changes for the low- and high-recovery cases because they do not result in a significant change in the soda ash dose. For example, we observe nearly no change in LCOW for case 4, corresponding to the low-recovery seawater case, because only recarbonation is required to control calcium carbonate scaling, which comprises a small fraction of the LCOW.

This analysis indicates that there could be substantial benefits in process changes and innovations that allow higher maximum allowable scaling tendencies because they can replace or reduce expensive chemical precipitation pretreatment needs such as soda ash softening. These process changes could include the addition of antiscalants,[40,113,114] membrane material advancements for improved scaling resistance,[3,115] electrified membranes for scaling control,[116,117] and alternative operational strategies that could potentially avoid induction time, such as semibatch/batch RO[42] or reverse flow RO.[118−120]

4. CONCLUSIONS

Numerous emerging technologies for high-recovery desalination have been proposed in the literature. However, due to the difficulty of estimating pretreatment needs and predicting mineral scaling in multicomponent feed sources, studies often overlook pretreatment and mineral scaling and simplify analyses to high recovery for sodium chloride feeds. We present a modeling framework for integrating accurate water

chemistry surrogate models with process-scale optimization of full treatment trains with mineral scaling control. Our framework enables the estimation of the pretreatment, cost, and operational requirements required to push conventional desalination treatment trains to high recoveries while maintaining a feasible operation. To the best of our knowledge, this study is the first to perform a cost optimization that directly accounts for both pretreatment requirements and mineral scale prediction for high-recovery desalination of multicomponent feed sources.

At high recovery rates, pretreatment costs for scaling control can significantly increase the costs of brackish and seawater desalination. Our results show that adding soda ash to prevent gypsum scaling in brackish and seawater at high recoveries above 67 and 74% in the third regime, respectively, can nearly double the overall cost of treatment, suggesting that future work should explore alternative precipitation agents. Additionally, using recarbonation to control calcium carbonate scaling in brackish water accounts for over 25% of the cost, suggesting that future work should also explore alternative pH and scaling control methods. Critically, cost optimization of the full treatment train revealed that beyond chemical addition for scaling control strategies that change the design of the RO system to minimize scaling can substantially reduce overall pretreatment requirements and process costs.

The presented results highlight the importance of a holistic approach to process optimization, where pretreatment and primary treatment processes are designed synergistically to achieve a cost-optimal operation. Although the analysis in this work was performed using steady-state models and depended on equilibrium-based scaling tendencies, the presented optimization framework can be extended to dynamic process design and kinetics, where scaling control targets such as the induction time could be considered. Critically, this framework provides a rapid, accurate, and detailed approach to process design that has significant improvements over existing methods that typically rely on manually selecting process design specifications, testing if scaling would occur, and readjusting pretreatment based on the results. Our framework can be applied to more comprehensively evaluate and support research and development for other emerging high-recovery desalination technologies and treatment trains.

ASSOCIATED CONTENT

Supporting Information

The Supporting Information is available free of charge at https://pubs.acs.org/doi/10.1021/acsestengg.3c00537.

> Additional modeling details, including model equations, costing information, algorithms for adaptive sampling, tables for additional surrogate modeling results, and figures showing additional results for operating parameters (PDF)

> Detailed analysis results, including cost breakdowns (ZIP)

AUTHOR INFORMATION

Corresponding Author

Timothy V. Bartholomew − *National Energy Technology Laboratory (NETL), Pittsburgh, Pennsylvania 15236, United States;* orcid.org/0000-0001-5091-7923; Phone: (412)386-9164; Email: timothy.bartholomew@netl.doe.gov

Authors

Oluwamayowa O. Amusat − *Lawrence Berkeley National Laboratory (LBNL), Berkeley, California 94720, United States*

Adam A. Atia − *National Energy Technology Laboratory (NETL), Pittsburgh, Pennsylvania 15236, United States; NETL Support Contractor, Pittsburgh, Pennsylvania 15236, United States*

Alexander V. Dudchenko − *SLAC National Accelerator Laboratory, Menlo Park, California 94025, United States;* orcid.org/0000-0002-4808-6195

Complete contact information is available at:
https://pubs.acs.org/10.1021/acsestengg.3c00537

Author Contributions

CRediT: **Oluwamayowa O Amusat** conceptualization, formal analysis, methodology, software, visualization, writing-original draft, writing-review & editing; **Adam A Atia** conceptualization, methodology, software, writing-original draft, writing-review & editing; **Alexander V Dudchenko** methodology, software, visualization, writing-original draft, writing-review & editing; **Timothy V Bartholomew** conceptualization, methodology, software, supervision, writing-original draft, writing-review & editing.

Notes

The authors declare no competing financial interest.

ACKNOWLEDGMENTS

REFERENCES

(1) Matin, A.; Rahman, F.; Shafi, H. Z.; Zubair, S. M. Scaling of reverse osmosis membranes used in water desalination: Phenomena, impact, and control; future directions. *Desalination* **2019**, *455*, 135−157.

(2) Turek, M.; Mitko, K.; Piotrowski, K.; Dydo, P.; Laskowska, E.; Jakóbik-Kolon, A. Prospects for high water recovery membrane desalination. *Desalination* **2017**, *401*, 180−189.

(3) Tong, T.; Wallace, A. F.; Zhao, S.; Wang, Z. Mineral scaling in membrane desalination: Mechanisms, mitigation strategies, and feasibility of scaling-resistant membranes. *J. Membr. Sci.* **2019**, *579*, 52−69.

(4) Shirazi, S.; Lin, C.-J.; Chen, D. Inorganic fouling of pressure-driven membrane processes—A critical review. *Desalination* **2010**, *250*, 236−248.

(5) MacAdam, J.; Jarvis, P. Water-Formed Scales and Deposits: Types, Characteristics, and Relevant Industries. In *Mineral Scales and Deposits*; Amjad, Z.; Demadis, K. D., Eds.; Elsevier: Amsterdam, 2015; Chapter 1, pp 3−23.

(6) Ruiz-García, A.; Feo-García, J. Estimation of maximum water recovery in RO desalination for different feedwater inorganic compositions. *Desalin. Water Treat.* **2017**, *70*, 34−45.

(7) Latteman, S. et al. *Development of an Environmental Impact Assessment and Decision Support System for Seawater Desalination Plants*; CRC Press Inc., 2010.

(8) Voutchkov, N. *Water Environment Federation, Water Reuse Association, Desalination engineering: Planning and Design*; McGraw-Hill: New York, 2013.

(9) Stanford, B. D.; Leising, J. F.; Bond, R. G.; Snyder, S. A. Inland Desalination: Current Practices, Environmental Implications, and Case Studies in Las Vegas, NV. In *Sustainability Science and Engineering*; Schäfer, A. I., Ed.; Elsevier, 2010; Chapter 11, pp 327−350.

(10) Antony, A.; Low, J. H.; Gray, S.; Childress, A. E.; Le-Clech, P.; Leslie, G. Scale formation and control in high pressure membrane water treatment systems: A review. *J. Membr. Sci.* **2011**, *383*, 1−16.

(11) Shah, K. M.; Billinge, I. H.; Chen, X.; Fan, H.; Huang, Y.; Winton, R. K.; Yip, N. Y. Drivers, challenges, and emerging technologies for desalination of high-salinity brines: A critical review. *Desalination* **2022**, *538*, No. 115827.

(12) Meijer, J. A. M.; Van Rosmalen, G. M. Solubilities and supersaturations of calcium sulfate and its hydrates in seawater. *Desalination* **1984**, *51*, 255−305.

(13) Pitzer, K. S. Thermodynamics of electrolytes. I. Theoretical basis and general equations. *J. Phys. Chem. A* **1973**, *77*, 268−277.

(14) Pitzer, K. S.; Mayorga, G. Thermodynamics of electrolytes. II. Activity and osmotic coefficients for strong electrolytes with one or both ions univalent. *J. Phys. Chem. A* **1973**, *77*, 2300−2308.

(15) Pitzer, K. S.; Mayorga, G. Thermodynamics of electrolytes. III. Activity and osmotic coefficients for 2−2 electrolytes. *J. Solution Chem.* **1974**, *3*, 539−546.

(16) Pitzer, K. S.; Peiper, J. C.; Busey, R. H. Thermodynamic Properties of Aqueous Sodium Chloride Solutions. *J. Phys. Chem. Ref. Data* **1984**, *13*, 1−102.

(17) Mistry, K. H.; Hunter, H. A.; Lienhard V, J. H. Effect of composition and nonideal solution behavior on desalination calculations for mixed electrolyte solutions with comparison to seawater. *Desalination* **2013**, *318*, 34−47.

(18) Chen, C.-C.; Evans, L. B. A local composition model for the excess Gibbs energy of aqueous electrolyte systems. *AIChE J.* **1986**, *32*, 444−454.

(19) Anderko, A.; Wang, P.; Rafal, M. Electrolyte solutions: from thermodynamic and transport property models to the simulation of industrial processes. *Fluid Phase Equilib.* **2002**, *194−197*, 123−142.

(20) Wang, P.; Anderko, A.; Young, R. D. A speciation-based model for mixed-solvent electrolyte systems. *Fluid Phase Equilib.* **2002**, *203*, 141−176.

(21) Wang, P.; Springer, R. D.; Anderko, A.; Young, R. D. Modeling phase equilibria and speciation in mixed-solvent electrolyte systems. *Fluid Phase Equilib.* **2004**, *222−223*, 11−17.

(22) Wang, P.; Anderko, A.; Springer, R. D.; Young, R. D. Modeling phase equilibria and speciation in mixed-solvent electrolyte systems: II. Liquid−liquid equilibria and properties of associating electrolyte solutions. *J. Mol. Liq.* **2006**, *125*, 37−44.

(23) Söhnel, O.; Mullin, J. W. Interpretation of crystallization induction periods. *J. Colloid Interface Sci.* **1988**, *123*, 43−50.

(24) He, S.; Oddo, J. E.; Tomson, M. B. The Nucleation Kinetics of Calcium Sulfate Dihydrate in NaCl Solutions up to 6 m and 90°C. *J. Colloid Interface Sci.* **1994**, *162*, 297−303.

(25) Shneidman, V. A.; Weinberg, M. C. Scaling properties of induction times in heterogeneous nucleation. *J. Chem. Phys.* **1991**, *95*, 9148−9150.

(26) Lancia, A.; Musmarra, D.; Prisciandaro, M. Measuring induction period for calcium sulfate dihydrate precipitation. *AIChE J.* **1999**, *45*, 390−397.

(27) Drak, A.; Glucina, K.; Busch, M.; Hasson, D.; Laîne, J.-M.; Semiat, R. Laboratory technique for predicting the scaling propensity of RO feed waters. *Desalination* **2000**, *132*, 233−242.

(28) McCool, B. C.; Rahardianto, A.; Faria, J.; Kovac, K.; Lara, D.; Cohen, Y. Feasibility of reverse osmosis desalination of brackish agricultural drainage water in the San Joaquin Valley. *Desalination* **2010**, *261*, 240−250.

(29) Rahardianto, A.; Shih, W.-Y.; Lee, R.-W.; Cohen, Y. Diagnostic characterization of gypsum scale formation and control in RO membrane desalination of brackish water. *J. Membr. Sci.* **2006**, *279*, 655−668.

(30) Shih, W.-Y.; Rahardianto, A.; Lee, R.-W.; Cohen, Y. Morphometric characterization of calcium sulfate dihydrate (gypsum) scale on reverse osmosis membranes. *J. Membr. Sci.* **2005**, *252*, 253−263.

(31) Lin, N. H.; Shih, W.-Y.; Lyster, E.; Cohen, Y. Crystallization of calcium sulfate on polymeric surfaces. *J. Colloid Interface Sci.* **2011**, *356*, 790−797.

(32) Uchymiak, M.; Lyster, E.; Glater, J.; Cohen, Y. Kinetics of gypsum crystal growth on a reverse osmosis membrane. *J. Membr. Sci.* **2008**, *314*, 163−172.

(33) Rahardianto, A.; McCool, B. C.; Cohen, Y. Reverse Osmosis Desalting of Inland Brackish Water of High Gypsum Scaling Propensity: Kinetics and Mitigation of Membrane Mineral Scaling. *Environ. Sci. Technol.* **2008**, *42*, 4292−4297.

(34) Bartman, A. R.; Lyster, E.; Rallo, R.; Christofides, P. D.; Cohen, Y. Mineral scale monitoring for reverse osmosis desalination via real-time membrane surface image analysis. *Desalination* **2011**, *273*, 64−71.

(35) Lee, T.; Choi, J. Y.; Cohen, Y. Gypsum scaling propensity in semi-batch RO (SBRO) and steady-state RO with partial recycle (SSRO-PR). *J. Membr. Sci.* **2019**, *588*, No. 117106.

(36) Benecke, J.; Haas, M.; Baur, F.; Ernst, M. Investigating the development and reproducibility of heterogeneous gypsum scaling on

reverse osmosis membranes using real-time membrane surface imaging. *Desalination* **2018**, *428*, 161−171.

(37) Hasson, D.; Drak, A.; Semiat, R. Inception of CaSO4 scaling on RO membranes at various water recovery levels. *Desalination* **2001**, *139*, 73−81.

(38) Karabelas, A. J.; Karanasiou, A.; Mitrouli, S. T. Incipient membrane scaling by calcium sulfate during desalination in narrow spacer-filled channels. *Desalination* **2014**, *345*, 146−157.

(39) Li, X.; Hasson, D.; Shemer, H. Flow conditions affecting the induction period of CaSO4 scaling on RO membranes. *Desalination* **2018**, *431*, 119−125.

(40) Hasson, D.; Drak, A.; Semiat, R. Induction times induced in an RO system by antiscalants delaying CaSO4 precipitation. *Desalination* **2003**, *157*, 193−207.

(41) Oshchepkov, M. S.; Pervov, A. G.; Golovesov, V. A.; Rudakova, G.Ya.; Kamagurov, S. D.; Tkachenko, S. V.; Andrianov, A. P.; Popov, K. I. Use of a Fluorescent Antiscalant to Investigate Scaling of Reverse Osmosis Membranes. *Membr. Membr. Technol.* **2019**, *1*, 254−266.

(42) Warsinger, D. M.; Tow, E. W.; Maswadeh, L. A.; Connors, G. B.; Swaminathan, J.; Lienhard V, J. H. Inorganic fouling mitigation by salinity cycling in batch reverse osmosis. *Water Res.* **2018**, *137*, 384−394.

(43) Islam, M. R.; Hsieh, I.-M.; Lin, B.; Thakur, A. K.; Chen, C.-C.; Malmali, M. Molecular thermodynamics for scaling prediction: Case of membrane distillation. *Sep. Purif. Technol.* **2021**, *276*, No. 119231.

(44) Ling, B.; Battiato, I. Rough or wiggly? Membrane topology and morphology for fouling control. *J. Fluid Mech.* **2019**, *862*, 753−780.

(45) Ahdab, Y. D.; Thiel, G. P.; Böhlke, J. K.; Stanton, J.; Lienhard, J. H. Minimum energy requirements for desalination of brackish groundwater in the United States with comparison to international datasets. *Water Res.* **2018**, *141*, 387−404.

(46) Lyster, E.; Cohen, Y. Numerical study of concentration polarization in a rectangular reverse osmosis membrane channel: Permeate flux variation and hydrodynamic end effects. *J. Membr. Sci.* **2007**, *303*, 140−153.

(47) Freiburger, A. P.; Molins, S.; Buckley, H. L. A One-Dimensional Reactive Transport Model of Geochemical Scaling in Reverse Osmosis Desalination. *Soc. Sci. Res. Network* **2022**, No. 4124149.

(48) Thiel, G. P.; Lienhard, J. H. Treating produced water from hydraulic fracturing: Composition effects on scale formation and desalination system selection. *Desalination* **2014**, *346*, 54−69.

(49) Ruiz-García, A.; de la Nuez-Pestana, I. A computational tool for designing BWRO systems with spiral wound modules. *Desalination* **2018**, *426*, 69−77.

(50) Edalat, A.; Hoek, E. M. V. Techno-Economic Analysis of RO Desalination of Produced Water for Beneficial Reuse in California. *Water* **2020**, *12*, 1850.

(51) Micari, M.; Cipollina, A.; Tamburini, A.; Moser, M.; Bertsch, V.; Micale, G. Techno-economic analysis of integrated processes for the treatment and valorisation of neutral coal mine effluents. *J. Cleaner Prod.* **2020**, *270*, No. 122472.

(52) Morgante, C.; Vassallo, F.; Xevgenos, D.; Cipollina, A.; Micari, M.; Tamburini, A.; Micale, G. Valorisation of SWRO brines in a remote island through a circular approach: Techno-economic analysis and perspectives. *Desalination* **2022**, *542*, No. 116005.

(53) Jafari, M.; Vanoppen, M.; van Agtmaal, J. M. C.; Cornelissen, E. R.; Vrouwenvelder, J. S.; Verliefde, A.; van Loosdrecht, M. C. M.; Picioreanu, C. Cost of fouling in full-scale reverse osmosis and nanofiltration installations in the Netherlands. *Desalination* **2021**, *500*, No. 114865.

(54) Ruiz-García, A.; Feo-García, J. Antiscalant cost and maximum water recovery in reverse osmosis for different inorganic composition of groundwater. *Desalin. Water Treat.* **2017**, *73*, 46−53.

(55) Cohen, Y. Membrane Desalination of Agricultural Drainage Water: Water Recovery Enhancement and Brine Minimization, 2008. https://escholarship.org/uc/item/926140wt.

(56) Bartholomew, T. V.; Siefert, N. S.; Mauter, M. S. Cost Optimization of Osmotically Assisted Reverse Osmosis. *Environ. Sci. Technol.* **2018**, *52*, 11813−11821.

(57) Bartholomew, T. V.; Dudchenko, A. V.; Siefert, N. S.; Mauter, M. S. Cost optimization of high recovery single stage gap membrane distillation. *J. Membr. Sci.* **2020**, *611*, No. 118370.

(58) Dudchenko, A. V.; Bartholomew, T. V.; Mauter, M. S. Cost optimization of multi-stage gap membrane distillation. *J. Membr. Sci.* **2021**, *627*, No. 119228.

(59) Atia, A. A.; Yip, N. Y.; Fthenakis, V. Pathways for minimal and zero liquid discharge with enhanced reverse osmosis technologies: Module-scale modeling and techno-economic assessment. *Desalination* **2021**, *509*, No. 115069.

(60) Atia, A. A.; Allen, J.; Young, E.; Knueven, B.; Bartholomew, T. V. Cost optimization of low-salt-rejection reverse osmosis. *Desalination* **2023**, *551*, No. 116407.

(61) Process Simulation and Modeling Software; OLI Systems, Inc., 2023, https://www.olisystems.com/.

(62) Parkhurst, D. L.; Appelo, C. A. J. *Description of Input and Examples for PHREEQC version 3: A Computer Program for Speciation, Batch-Reaction, One-Dimensional Transport, and Inverse Geochemical Calculations*; U.S. Geological Survey, 2013. DOI: 10.3133/tm6A43.

(63) WaterTAP Contributors. WaterTAP: An Open-Source Water Treatment Model Library. Version 0.6. Sponsored by California Energy Commission, National Alliance for Water Innovation, and USDOE, 2023. https://github.com/watertap-org/watertap.

(64) Davenport, D. M.; Deshmukh, A.; Werber, J. R.; Elimelech, M. High-Pressure Reverse Osmosis for Energy-Efficient Hypersaline Brine Desalination: Current Status, Design Considerations, and Research Needs. *Environ. Sci. Technol. Lett.* **2018**, *5*, 467−475.

(65) Mistry, K. H.; Lienhard V, J. H. Effect of Nonideal Solution Behavior on Desalination of a Sodium Chloride Solution and Comparison to Seawater. *J. Energy Resour. Technol.* **2013**, *135*, No. 042003.

(66) Dudchenko, A. V.; Bartholomew, T. V.; Mauter, M. S. High-impact innovations for high-salinity membrane desalination. *Proc. Natl. Acad. Sci. U.S.A.* **2021**, *118*, No. e2022196118.

(67) Davenport, D. M.; Ritt, C. L.; Verbeke, R.; Dickmann, M.; Egger, W.; Vankelecom, I. F. J.; Elimelech, M. Thin film composite membrane compaction in high-pressure reverse osmosis. *J. Membr. Sci.* **2020**, *610*, No. 118268.

(68) Wu, J.; Jung, B.; Anvari, A.; Im, S.; Anderson, M.; Zheng, X.; Jassby, D.; Kaner, R. B.; Dlamini, D.; Edalat, A.; Hoek, E. M. V. Reverse osmosis membrane compaction and embossing at ultra-high pressure operation. *Desalination* **2022**, *537*, No. 115875.

(69) Shammas, N. K. Coagulation and Flocculation. In *Physicochemical Treatment Processes*; Wang, L. K.; Hung, Y.-T.; Shammas, N. K., Eds.; Humana Press: Totowa, NJ, 2005; pp 103−139.

(70) Wang, L. K.; Wu, J. S.; Shammas, N. K.; Vaccari, D. A. Recarbonation and Softening. In *Physicochemical Treatment Processes*; Wang, L. K.; Hung, Y.-T.; Shammas, N. K., Eds.; Humana Press: Totowa, NJ, 2005; pp 199−228.

(71) McGivney, W.; Kawamura, S. *Cost Estimating Manual for Water Treatment Facilities*; John Wiley & Sons, 2008. http://onlinelibrary.wiley.com/book/10.1002/9780470260036.

(72) Crittenden, J. C.; Trussell, R. R.; Hand, D. W.; Howe, K. J.; Tchobanoglous, G. *MWH's Water Treatment: Principles and Design*; John Wiley & Sons, 2012.

(73) Al-Mutaz, I. S.; Al-Ghunaimi, M. A. In *pH Control in Water Treatment Plant by the Addition of Carbon Dioxide*, The IDA World Congress on Desalination and Water Reuse, Bahrain, 2001; pp 1−12.

(74) Cost and Maintenance Reduction with CO2 to Replace Sulfuric Acid for pH Control at Steel Dynamics, Inc. (Butler, IN), Treatment Plant Operator, 2015. https://www.tpomag.com/uploads/downloads/P-40-4099_CO%C2%B2_replaces_Sulfuric_for_pH_control_at_SDI_180119_134148.pdf.

(75) Salvador Cob, S.; Beaupin, C.; Hofs, B.; Nederlof, M. M.; Harmsen, D. J. H.; Cornelissen, E. R.; Zwijnenburg, A.; Genceli Güner, F. E.; Witkamp, G. J. Silica and silicate precipitation as limiting factors in high-recovery reverse osmosis operations. *J. Membr. Sci.* **2012**, *423−424*, 1−10.

(76) Dzombak, D. A.; Morel, F. M. *Surface Complexation Modeling: Hydrous Ferric Oxide*; John Wiley & Sons, 1991.

(77) McKeague, J. A.; Cline, M. G. Silica in Soils. In *Advances in Agronomy*; Norman, A. G., Ed.; Academic Press, 1963; pp 339−396.

(78) The WaterTAP Development Repository, 2022. https://github.com/watertap-org/watertap.

(79) Lee, A.; Ghouse, J. H.; Chen, Q.; Eslick, J. C.; Siirola, J. D.; Grossman, I. E.; Miller, D. C. A Flexible Framework and Model Library for Process Simulation, Optimization and Control. In *Computer Aided Chemical Engineering*; Eden, M. R.; Ierapetritou, M. G.; Towler, G. P., Eds.; Elsevier, 2018; pp 937−942.

(80) Lee, A.; Ghouse, J. H.; Eslick, J. C.; Laird, C. D.; Siirola, J. D.; Zamarripa, M. A.; Gunter, D.; Shinn, J. H.; Dowling, A. W.; Bhattacharyya, D.; Biegler, L. T.; Burgard, A. P.; Miller, D. C. The IDAES process modeling framework and model library—Flexibility for process simulation and optimization. *J. Adv. Manuf. Process.* **2021**, *3*, No. e10095.

(81) The IDAES Process Systems Engineering Framework, 2022. https://github.com/IDAES/idaes-pse.

(82) Hart, W. E.; Watson, J.-P.; Woodruff, D. L. Pyomo: modeling and solving mathematical programs in Python. *Math. Program. Comput.* **2011**, *3*, 219−260.

(83) Bynum, M. L.; Hackebeil, G. A.; Hart, W. E.; Laird, C. D.; Nicholson, B. L.; Siirola, J. D.; Watson, J.-P.; Woodruff, D. L. *Pyomo—Optimization Modeling in Python*; Springer International Publishing: Cham, 2021. DOI: 10.1007/978-3-030-68928-5.

(84) Sharqawy, M. H.; Lienhard, J. H.; Zubair, S. M. Thermophysical properties of seawater: a review of existing correlations and data. *Desalin. Water Treat.* **2010**, *16*, 354−380.

(85) Nayar, K. G.; Sharqawy, M. H.; Banchik, L. D.; Lienhard, J. H. Thermophysical properties of seawater: A review and new correlations that include pressure dependence. *Desalination* **2016**, *390*, 1−24.

(86) Lencka, M. M.; Springer, R. D.; Wang, P.; Anderko, A. Modeling Mineral Scaling in Oil and Gas Environments up to Ultra High Pressures and Temperatures. In *Corrosion*; OnePetro, 2018.

(87) Scaling Tendencies—wiki.olisystems.com, 2023. https://wiki.olisystems.com/wiki/Scaling_Tendencies.

(88) McBride, K.; Sundmacher, K. Overview of Surrogate Modeling in Chemical Process Engineering. *Chem. Ing. Tech.* **2019**, *91*, 228−239.

(89) PySMO: Python-Based Surrogate Modelling Objects—IDAES v1.13.2, 2023. https://idaes-pse.readthedocs.io/en/stable/explanations/modeling_extensions/surrogate/pysmo/index.html.

(90) Wilson, Z. T.; Sahinidis, N. V. The ALAMO approach to machine learning. *Comput. Chem. Eng.* **2017**, *106*, 785−795.

(91) Jones, D. R.; Schonlau, M.; Welch, W. J. Efficient Global Optimization of Expensive Black-Box Functions. *J. Glob. Optim.* **1998**, *13*, 455−492.

(92) Sobester, A.; Forrester, A.; Keane, A. *Engineering Design via Surrogate Modelling: A Practical Guide*; John Wiley & Sons, 2008.

(93) Díaz-Manríquez, A.; Toscano-Pulido, G.; Gómez-Flores, W. In *On the Selection of Surrogate Models in Evolutionary Optimization Algorithms*, 2011 IEEE Congress of Evolutionary Computation (CEC), IEEE, 2011; pp 2155−2162.

(94) Mckay, M. D.; Beckman, R. J.; Conover, W. J. A Comparison of Three Methods for Selecting Values of Input Variables in the Analysis of Output From a Computer Code. *Technometrics* **2000**, *42*, 55−61.

(95) Wong, T.-T.; Luk, W.-S.; Heng, P.-A. Sampling with Hammersley and Halton Points. *J. Graphics Tools* **1997**, *2*, 9−24.

(96) Swiler, L.; Slepoy, R.; Giunta, A. In *Evaluation of Sampling Methods in Constructing Response Surface Approximations*, 47th AIAA/ASME/ASCE/AHS/ASC Structures, Structural Dynamics, and Materials Conference, American Institute of Aeronautics and Astronautics, 2006.

(97) Regis, R. G. Stochastic radial basis function algorithms for large-scale optimization involving expensive black-box objective and constraint functions. *Comput. Oper. Res.* **2011**, *38*, 837−853.

(98) Baker, R. J.; van Leeuwen, J. H.; White, D. J. *Applications for Reuse of Lime Sludge from Water Softening*; Iowa State University, 2005.

(99) Gumerman, R. C.; Culp, R. L.; Hansen, S. P. *Estimating Water Treatment Costs: Vol. 2. Cost Curves Applicable to 1 to 200 mgd Treatment Plants*, US EPA, EPA-600/2-79-162b; Drinking Water Research Division, Municipal Environmental Research Laboratory, 1979.

(100) Siddiqui, A.; Lehmann, S.; Haaksman, V.; Ogier, J.; Schellenberg, C.; van Loosdrecht, M. C. M.; Kruithof, J. C.; Vrouwenvelder, J. S. Porosity of spacer-filled channels in spiral-wound membrane systems: Quantification methods and impact on hydraulic characterization. *Water Res.* **2017**, *119*, 304−311.

(101) Lin, W.; Wang, Q.; Sun, L.; Wang, D.; Cabrera, J.; Li, D.; Hu, L.; Jiang, G.; Wang, X.; Huang, X. The critical role of feed spacer channel porosity in membrane biofouling: Insights and implications. *J. Membr. Sci.* **2022**, *649*, No. 120395.

(102) Miara, A.; Talmadge, M.; Sitterley, K.; Evans, A.; Huang, Z.; Macknick, J.; McCall, J.; Kurup, P.; Akar, S.; Van Allsburg, K.; Stokes-Draut, J.; Bartholomew, T.; Lee, A.; Gingerich, D. In *WaterTAP3 (The Water Technoeconomic Assessment Pipe-Parity Platform)*, Computer Software Version 0.0.2; USDOE Office of Energy Efficiency and Renewable Energy (EERE), Energy Efficiency Office, Advanced Manufacturing Office: Golden, CO, 2021.

(103) Faulconbridge, G.; Holton, K.; Davey, J. Britain Tells its Food Industry to Prepare for CO2 Price Shock, Reuters, 2021. https://www.reuters.com/world/uk/uk-pay-tens-millions-get-carbon-dioxide-pumping-again-2021-09-22/.

(104) Unstable Market for CO2 Increases Costs to Treat Drinking Water, Jamestown Sun, 2022. https://www.jamestownsun.com/news/unstable-market-for-co2-increases-costs-to-treat-drinking-water.

(105) Crittenden, J. C.; Trussell, R. R.;et al. Reverse Osmosis. In *MWH's Water Treatment: Principles and Design*; John Wiley & Sons, 2012.

(106) Thompson, J. F. Membrane Mineral Scaling and its Mitigation in Reverse Osmosis Desalination of Brackish Water. Ph.D. Dissertation, University of California: Los Angeles, 2017.

(107) Birnhack, L.; Voutchkov, N.; Lahav, O. Fundamental chemistry and engineering aspects of post-treatment processes for desalinated water—A review. *Desalination* **2011**, *273*, 6−22.

(108) Sharma, J. R. Development of a Preliminary Cost Estimation Method For Water Treatment Plants, 2010. https://rc.library.uta.edu/uta-ir/handle/10106/4924.

(109) Sharma, J. R.; Najafi, M.; Qasim, S. R. Preliminary Cost Estimation Models for Construction, Operation, and Maintenance of Water Treatment Plants. *J. Infrastruct. Syst.* **2013**, *19*, 451−464.

(110) Tong, T.; Elimelech, M. The Global Rise of Zero Liquid Discharge for Wastewater Management: Drivers, Technologies, and Future Directions. *Environ. Sci. Technol.* **2016**, *50*, 6846−6855.

(111) Kulkarni, S. A.; Kadam, S. S.; Meekes, H.; Stankiewicz, A. I.; ter Horst, J. H. Crystal Nucleation Kinetics from Induction Times and Metastable Zone Widths. *Cryst. Growth Des.* **2013**, *13*, 2435−2440.

(112) Brandel, C.; ter Horst, J. H. Measuring induction times and crystal nucleation rates. *Faraday Discuss.* **2015**, *179*, 199−214.

(113) Popov, K.; Rudakova, G.; Larchenko, V.; Tusheva, M.; Kamagurov, S.; Dikareva, J.; Kovaleva, N. A Comparative Performance Evaluation of Some Novel "Green" and Traditional Antiscalants in Calcium Sulfate Scaling. *Adv. Mater. Sci. Eng.* **2016**, *2016*, No. e7635329.

(114) Yu, W.; Song, D.; Chen, W.; Yang, H. Antiscalants in RO membrane scaling control. *Water Res.* **2020**, *183*, No. 115985.

(115) Kang, G.-d.; Cao, Y. Development of antifouling reverse osmosis membranes for water treatment: A review. *Water Res.* **2012**, *46*, 584−600.

(116) Duan, W.; Dudchenko, A.; Mende, E.; Flyer, C.; Zhu, X.; Jassby, D. Electrochemical mineral scale prevention and removal on electrically conducting carbon nanotube—polyamide reverse osmosis membranes. *Environ. Sci.: Processes Impacts* **2014**, *16*, 1300−1308.

(117) Tang, L.; Iddya, A.; Zhu, X.; Dudchenko, A. V.; Duan, W.; Turchi, C.; Vanneste, J.; Cath, T. Y.; Jassby, D. Enhanced Flux and Electrochemical Cleaning of Silicate Scaling on Carbon Nanotube-Coated Membrane Distillation Membranes Treating Geothermal Brines. *ACS Appl. Mater. Interfaces* **2017**, *9*, 38594−38605.

(118) Pomerantz, N.; Ladizhansky, Y.; Korin, E.; Waisman, M.; Daltrophe, N.; Gilron, J. Prevention of Scaling of Reverse Osmosis Membranes by "Zeroing" the Elapsed Nucleation Time. Part I. Calcium Sulfate. *Ind. Eng. Chem. Res.* **2006**, *45*, 2008−2016.

(119) Gilron, J.; Waisman, M.; Daltrophe, N.; Pomerantz, N.; Milman, M.; Ladizhansky, I.; Korin, E. Prevention of precipitation fouling in NF/RO by reverse flow operation. *Desalination* **2006**, *199*, 29−30.

(120) Uchymiak, M.; Bartman, A. R.; Daltrophe, N.; Weissman, M.; Gilron, J.; Christofides, P. D.; Kaiser, W. J.; Cohen, Y. Brackish water reverse osmosis (BWRO) operation in feed flow reversal mode using an ex situ scale observation detector (EXSOD). *J. Membr. Sci.* **2009**, *341*, 60−66.